NATURAL INFRASTRUCTURE - THE VALUE OF GREEN

by

SWATY KAJARIA

(Under the Direction of Susana Ferreira and Yukiko Hashida)

ABSTRACT

Coastal environments are dynamic systems where natural processes, human development, and economic decisions interact in complex ways. My research sits at the intersection of environmental economics, spatial analysis, and remote sensing focusing on how coastal ecosystems influence economic outcomes and how communities respond to environmental change. Under the broader theme of natural infrastructure, my dissertation explores how the presence of mangrove forests shapes perceptions of environmental amenities and is reflected in housing market behavior. The dissertation also develops a methodology to address the absence of historical data on mangrove extent, using satellite imagery and cloud-based computing to generate spatial estimates of past mangrove coverage for long-term analysis.

INDEX WORDS: Coastal Protection, Environmental Valuation, Google Earth Engine,
Hedonic Pricing, Housing Market, Hurricane Irma, Land Cover Change,
Machine Learning, Mangrove Ecosystems, Natural Infrastructure,
Nonmarket Valuation, Remote Sensing, Spatial Analysis

NATURAL INFRASTRUCTURE - THE VALUE OF GREEN

by

SWATY KAJARIA

B.E., University of Pune, India, 2003

P.G.D.F.M., Indian Institute of Forest Management, Bhopal, India, 2015

M.N.R., University of Georgia, 2025

A Dissertation Submitted to the Graduate Faculty of The University of Georgia in Partial

Fulfillment of the Requirements for the Degree

DOCTOR OF PHILOSOPHY

ATHENS, GEORGIA

2025

© 2025

Swaty Kajaria

All Rights Reserved

NATURAL INFRASTRUCTURE - THE VALUE OF GREEN

by

SWATY KAJARIA

Major Professor: Susana Ferreira

Yukiko Hashida

Committee: Craig Landry

Jeffrey Hepinstall Cymerman

Electronic Version Approved:

Ron Walcott Vice Provost for Graduate Education and Dean of the Graduate School The University of Georgia August 2025

DEDICATION

To my mother, Santosh, whose unwavering support anchors me, and my daughter, Mishka, whose quiet strength across distance inspires me.

ACKNOWLEDGEMENTS

I am grateful to Dr. Susana Ferreira for her guidance, insights and unwavering support throughout this journey. I am thankful to Dr. Yukiko Hashida for her feedback, direction and support throughout the research process. I sincerely thank my committee members, Dr. Craig Landry and Dr. Jeffrey Hepinstall Cymerman, for their reviews and input.

TABLE OF CONTENTS

Chapter 1 Introduction	1
Chapter 2 Nature's Shield: Deciphering Mangroves' Influence on Property Value D	ynamics in
the Wake of Hurricane Irma	4
2.1 Introduction	4
2.2 Study Area	9
2.3 Empirical Strategy	11
2.4 Data & Descriptive Statistics	18
2.5 Results	21
2.6 Discussion	25
2.7 Conclusion	27
Chapter 3 Let 'Em Grow: Do Florida Coastal Property Owners Value Mangroves? .	48
3.1 Introduction	48
3.2 Study Area	52
3.3 Empirical Strategy	53
3.4 Data & Descriptive Statistics	57
3.5 Results	59
3.6 Discussion	61

Chapter 4 Shoreline Wonders: Navigating Mangroves with Geographic Information Systems	71
4.1 Introduction	71
4.2 Study Area	73
4.3 Data Sources	75
4.4 Methodology	76
4.5 Experimental Setup	80
4.6 Results	82
4.7 Discussion	84
Chapter 5 Conclusion	94

LIST OF TABLES

Table 2.1: Spatial and Temporal Distribution of Sales Transactions (2015-2019) within 1K	
buffer	28
Table 2.2: Summary Statistics for within 1K buffer and for repeat sales houses	29
Table 2.3: Property Fixed Effects Regression Output within 1K	30
Table 2.4: Robustness Check with Property Fixed Effects Regression Output within 2K	31
Table 2.5: Placebo Test	32
Table 2.6: Neighbourhood Fixed Effects Regression Output within 1K buffer	33
Table 2.7: Alternative Protection Measure Based on Relative Proximity	45
Table 2.8: Neighbourhood Fixed Effects Regression Output	46
Table 3.1: Correspondence of Mangrove Extent Years to House Sale Years	63
Table 3.2: Descriptive Statistics	63
Table 3.3: Property Fixed Effects Regression	64
Table 3.4: Pooled Regression Output using Proximity measure only	68
Table 3.5: Pooled Regression Output for Pinellas Conty using area and viewshed measure.	69
Table 4.1: Indices Computed	86
Table 4.2: Model Outcome	86

LIST OF FIGURES

Figure 1.1: Mangrove swamp, partly underwater
Figure 2.1: Lee County Single Family Sales from 2015 to 2019
Figure 2.2: Proximity-based mangrove protection may overstate actual protection
Figure 2.3: Determining protection status based on the relative positions of houses, mangroves,
and the ocean
Figure 2.4: Directional Protection Concept and GIS-Based Implementation
Figure 2.5: Spatial Distribution of Properties Relative to Coastal Features in Lee County 38
Figure 2.6: Mangrove extent before and after Hurricane Irma
Figure 2.7: Event Study Plot
Figure 2.8: Pre-trend of the two group
Figure 2.9: Mangroves & Ocean in the same direction, properties are protected
Figure 2.10: Mangroves & Ocean in the same direction, properties are not protected
Figure 2.11: Mangroves & Ocean in opposite direction, properties are not protected 44
Figure 3.1: Study Area - Pinellas and Hillsborough County, Florida
Figure 3.2: Visibility analysis for a representative property, showing buffer, viewshed,
mangroves, and visible mangrove extent
Figure 3.3: Repeat sales within 2K buffer
Figure 4.1: Study Area: Tampa Bay, Southwest Florida
Figure 4.2: Block Diagram of Mangroves Extent Mapping

Figure 4.3: Spatial distribution of (a) core mangrove areas, (b) non-mangrove regions, and (c)	
final training labels used for classification.	89
Figure 4.4: Pre-processed and Final Landsat surface reflectance image for the year 2020	90
Figure 4.5: Variable Importance from Random Forest Classifier	91
Figure 4.6: Predicted mangrove extent and GMW mangrove extent for 2020	92
Figure 4.7: Predicted mangroves year on year	93

Chapter 1

Introduction

As climate risks intensify and coastal populations grow, understanding the role of natural infrastructure in mitigating hazard exposure has become increasingly critical. Mangrove forests, found in tropical and subtropical intertidal zones, serve as natural buffers by reducing storm surge, stabilizing shorelines, and supporting biodiversity (Figure 1.1). Despite their recognized ecological importance, the protective services offered by mangroves remain underappreciated in economic analyses, largely due to the absence of market mechanisms to capture their value. This dissertation examines how households perceive and value mangrove protection through housing market behavior. It brings together insights from environmental economics, spatial analysis, and remote sensing to estimate the economic significance of mangroves in coastal Florida.

The first paper of this dissertation examines how the protective role of mangroves is perceived and valued by households in the aftermath of a major storm event. A key contribution of this study lies in the development of a novel proxy for directional protection, capturing whether mangroves are spatially positioned between a property and the coastline, and thus likely to offer physical protection from storm surge. The paper leverages the landfall of Hurricane Irma, a Category 4 hurricane that struck Florida in 2017, as an exogenous shock to estimate whether the presence of mangrove is capitalized into property prices. Using a difference-in-differences framework, the analysis compares price changes for homes with and without directional mangrove protection before and after the storm, offering a revealed-preference perspective on the perceived value of this ecosystem service.

The second chapter investigates how proximity to mangroves influences property values over a longer time horizon. Using a long-difference framework and property transaction data spanning two decades, the study explores whether and how housing markets have capitalized the presence of mangroves. The analysis draws on mangrove extent data from the Global Mangrove Watch for selected years and offers a preliminary perspective on the long-term economic relevance of coastal environmental amenities.

Recognizing that a major challenge in valuing natural infrastructure is the lack of historical spatial data, the third chapter addresses this gap by developing a methodology to generate past mangrove extent in Southwest Florida from the 1980s. This is achieved through the use of Landsat imagery, cloud-based computing, and machine learning classification techniques. The resulting dataset is intended to support future research on long-term mangrove dynamics and their ecosystem service contributions.

Together, these three chapters contribute to the literature on the economic and protective value of mangrove ecosystems by combining empirical analysis of housing market behavior with a methodological framework for estimating historical mangrove extent.



Figure 1.1: Mangrove swamp, partly underwater.

Photo credit: U.S. National Oceanic and Atmospheric Administration (public domain).

Chapter 2

Nature's Shield: Deciphering Mangroves' Influence on Property Value Dynamics in the

Wake of Hurricane Irma

2.1 Introduction

Coastal regions, increasingly vulnerable to climate change, face heightened risks from storm surge and hurricane-induced flooding, as evidenced by Hurricane Irma's extensive flood damage. On average, two hurricanes make landfall in the United States each year, predominantly along the Gulf and East Coasts (US EPA, 2016). These storms bring powerful winds and heavy rainfall, causing significant damage to infrastructure. The increasing frequency and intensity of such severe weather events highlight the urgent need for effective and cost-efficient hazard mitigation strategies. States like Florida are particularly vulnerable due to their unique geographic location, with extensive coastlines and being nearly surrounded by water. According to NOAA, coastal counties in the United States are home to 40 percent of the country's population, and these areas have experienced a 40 percent increase in population from 1970 to 2010 (National Oceanic and Atmospheric Administration, Office for Coastal Management, 2013). This rapid growth in vulnerable coastal zones underscores the importance of resilience planning, including the use of natural defenses.

As a natural coastal defense, mangrove forests, a wetland ecosystem situated between land and sea, are increasingly recognized for their ability to buffer storm surge, dissipate wave energy, and reduce flood risk (<u>Barbier, 2007</u>; Das & Vincent, 2009; Das & Crépin, 2013; <u>Narayan et al., 2019</u>; <u>Sun & Carson, 2020</u>) Despite their significance, these services frequently go unrecognized in economic planning and conservation efforts due to the absence of formal market mechanisms for

their valuation. This study examines whether and how these protective services provided by mangroves are capitalized into residential property values in Florida's coastal areas. Specifically, we ask: Do homes that are spatially protected by mangroves command higher prices, particularly in the aftermath of a major hurricane? We develop a novel spatial proxy that captures both the proximity and the directional positioning of mangroves relative to the ocean and individual properties. We link this protection proxy with property sales data and apply a difference-in-differences (DID) framework, using Hurricane Irma as an exogenous shock to identify the salience of mangrove protection in shaping property values.

A growing body of interdisciplinary work highlights the critical role of wetlands in providing natural protection. Occupying the transitional zone between land and sea, mangrove forests serve as buffers that reduce the impact of storm surges, high winds, and coastal flooding. An early influential provided compelling empirical evidence that mangrove belt width significantly reduced fatalities in villages near the coast during India's 1999 super cyclone, highlighting that vegetation itself, beyond elevation or topography, plays a key protective role (Das & Vincent, 2009). A follow-up study (Das & Crépin, 2013) extended this evidence by simulating how mangroves reduce wind velocity, finding notable reductions in structural damage even several kilometers inland. Beyond life-saving outcomes, mangrove forests have also been shown to enhance economic resilience. Studies (Del Valle et al., 2020; Hochard et al., 2019, 2021) used satellitederived nightlight data to analyze how mangrove coverage affects economic activity post-disaster. Del Valle et al. (2020) focusing on Central America, found that areas with mangrove belts of at least one kilometer experienced negligible short-run economic losses after hurricanes, while Hochard et al., in a global study of nearly 2,000 coastal communities, showed that mangrove buffers accelerated post-storm economic recovery.

Engineering-focused studies further support the value of mangroves as a protective asset. Zhang et al. (2012) using the Coastal and Estuarine Storm Tide model, demonstrated how mangrove vegetation attenuates storm surge, with effects varying nonlinearly by density and forest edge configuration. Tomiczek et al. (2021) synthesized physical experiments to emphasize how mangroves reduce wave energy and enhance coastal defense. These technical studies call for the integration of ecological and biophysical parameters into hazard mitigation planning. Parallel to this biophysical work, <u>Barbier (2007)</u> outlined two conceptual frameworks for ecosystem valuation of mangroves, the production function approach, which values services as inputs into economic outputs (e.g., fisheries), and the expected damage approach, which estimates how ecosystems reduce risk.

Barbier et al. (2013) and Barbier & Enchelmeyer (2014) exemplify how the ecological structure of coastal systems can be translated into quantifiable economic benefits. They applied storm surge modeling and expected damage functions to quantify the protective value of coastal wetlands across the Gulf Coast. Sun & Carson (2020) similarly utilized the expected damage function approach to assess the economic value of wetlands in mitigating damage resulting from 88 tropical storms and hurricanes that hit the United States between 1996 and 2016. In the context of Florida, Narayan et al. (2019) used an insurance industry catastrophe model to quantify the flood reduction benefits of mangroves. They compared surge-related property losses under scenarios with and without mangroves—both annually and during Hurricane Irma. Their results indicate that mangroves averted \$1.5 billion in property damage and annually flood risk by over 25%. While their analysis estimates avoided damage from a modeling and insurance perspective, our study is the first to apply a hedonic framework to assess how mangrove protection is reflected in housing prices and perceived by homeowners.

While mangrove and wetland ecosystems are increasingly recognized for their role in hazard mitigation (Danielsen et al., 2005; Das & Crépin, 2013; Das & Vincent, 2009; DasGupta & Shaw, 2017; Hochard et al., 2019, 2021; Menéndez et al., 2020; Zhang et al., 2012), much of the existing literature assesses these services at global or national scales. This broader framing, while highly informative, often masks the heterogeneity in exposure, ecological structure, and socioeconomic vulnerability across and within regions. In addition, while these studies have advanced our understanding of the protective value of the coastal ecosystems, they often do not directly capture how residents, who both benefit from and play a role in the conservation of these natural defenses, perceive and value them. A notable exception is Barbier (2008) who examined household participation in post-tsunami mangrove replanting efforts in Thailand, to highlight how socioeconomic factors such as income, property rights, and prior experience shape conservation decisions. Nonetheless, important gaps remain in understanding how natural defenses function at a finer spatial scale and whether and how their protective benefits are reflected in property values. Building on this need for granularity, our study links fine-scale spatial arrangements of mangroves to property values using real estate transaction data, an approach that remains underexplored. While past research has used buffer width or proximity measures to evaluate the protective role of mangroves (e.g., Das & Vincent, 2009; Das & Crépin, 2013), we introduce a novel protection proxy that accounts for both proximity to mangroves and their directional positioning relative to potential coastal exposure. This is motivated by findings from Alongi (2008), Temmerman et al. (2023) and Maza et al. (2017) which emphasize that mangrove protection is most effective when vegetation lies directly in the path of incoming storm surge or wave energy. By integrating these spatial dynamics, our study contributes a new, spatially explicit lens for understanding how natural coastal features influence property values and inform resilience planning.

We use hedonic property pricing models to identify the effect of mangrove protection on coastal property values. The hedonic property price approach has been widely used for the economic valuation of non-market goods, especially environmental amenities and disamenities. Applications in the coastal context include the valuation of beach nourishment (Gopalakrishnan et al., 2011), beach quality (Landry & Hindsley, 2021), dune renovations (Dundas, 2017a) and voluntary property buyout and acquisition (Hashida & Dundas, 2023). It has also been used to estimate coastal amenities and flood risk (Atreya et al., 2013; Atreya & Ferreira, 2015; Bakkensen et al., 2019; Bakkensen & Barrage, 2022; Bin, Kruse, et al., 2008; Kousky, 2019). Despite its broad application, the hedonic property pricing approach has not yet been applied to isolate the protective salience of mangroves, particularly at the property level. This gap likely stems from the complexity of disentangling protection benefits from other co-occurring services and disservices mangroves provide. In addition to protecting against storm surge, mangroves are associated with unpleasant odors and obstruction of oceanic views, which may also influence property values. The occurrence of a hurricane, however, increases the salience of mangroves' protective benefits and provides a quasi-experimental setting to study how these protective services are capitalized into property values. We employ a difference-in-differences (DID) framework, leveraging Hurricane Irma as an exogenous shock to assess the perceived value of natural protection provided by mangroves. Properties perceived to be protected by mangroves serve as the treated group, while comparable properties without such protection form the control group. By comparing pre- and post-hurricane price dynamics between these groups, we find that homes with protective mangrove coverage commanded at least a 7.6% price premium relative to similar unprotected properties. This approach parallels the work of Hallstrom & Smith (2005) who exploited a near-miss hurricane event in Lee County, Florida to examine how heightened storm risk perception affects property values.

Our work contributes to the growing literature on the economic valuation of ecological services provided by mangroves and wetlands. Previous valuation studies have estimated the role of mangroves in natural hazard mitigation in India (Das & Crépin, 2013; Das & Vincent, 2009), Thailand (Barbier, 2008) and the USA (Del Valle et al., 2020; Narayan et al., 2019; Sun & Carson, 2020). To the best of our knowledge, ours is the first hedonic pricing study to incorporate a fine-scale proxy that captures the spatial orientation between mangroves, the ocean, and individual properties. While prior works (Das & Vincent, 2009; Das & Crépin, 2013), have considered the direction of storm winds, coastline, and mangrove presence at broader spatial scales, we develop a spatially explicit, property-level measure of protective positioning that integrates these elements. Our study contributes to the literature on ecosystem service valuation by demonstrating how property-level spatial relationships between mangroves, coastlines, and homes influence housing prices. This approach offers a replicable method for valuing protective coastal features and provides actionable insights for conservation planning, coastal zoning, and climate adaptation.

2.2 Study Area

Lee County, located along Florida's Gulf Coast, experienced substantial damage from Hurricane Irma, a category 4 storm, in September 2017, providing relevant context for this analysis. Hurricane Irma caused widespread devastation across the state, with damages totaling \$50 billion (Federal Emergency Management Agency (FEMA), 2018), making it among the costliest hurricanes in U.S. history. In the five years following the disaster, Florida received more than \$5.58 billion in federal recovery funding. This assistance included over \$1 billion in grants provided by FEMA to aid individuals and households directly affected by the storm. Additionally,

nearly \$4 billion was disbursed through FEMA's National Flood Insurance Program to cover claims from policyholders. To support long-term recovery and resilience efforts, FEMA also allocated \$574 million in Public Assistance grants and \$5.7 million in Hazard Mitigation Assistance. These funds have played a critical role in rebuilding communities, restoring infrastructure, and reducing future disaster risks, showcasing the ongoing commitment to helping Florida recover from one of its most significant natural disasters.

Florida is home to an estimated 600,000 acres of mangrove forests, concentrated in its southern coastal regions. The three native species are red mangrove (Rhizophora mangle), black mangrove (Avicennia germinans), and white mangrove (Laguncularia racemosa), each have distinct ecological characteristics and occupy different zones within the intertidal environment. Red mangroves, typically found along the shoreline, are identifiable by their prop roots; black mangroves are located slightly inland and feature pneumatophores; and white mangroves occupy higher elevations with less prominent above-ground root structures. According to Iii & Walker (2016), the Pine Island Sound/Matlacha Pass sub-basin in Lee County contains an estimated 19,107 acres of mangroves. The presence of mangroves in Lee County played a crucial role during Hurricane Irma. These coastal forests acted as natural buffers, reducing the impact of storm surges and mitigating shoreline erosion (Narayan et al., 2019). Their complex root systems helped stabilize sediments and dissipate wave energy, thereby protecting inland areas from more severe damage. Post-storm assessments highlighted the resilience of mangroves and underscored their importance in coastal defence strategies. In the years following Hurricane Irma, restoration efforts in Lee County have been supported by organizations such as Keep Lee County Beautiful (KLCB) and the Sanibel-Captiva Conservation Foundation (SCCF), working to enhance and preserve mangrove habitats along the county's vulnerable coastlines.

According to 2020 U.S. Census Bureau data, Lee County has experienced significant population growth in recent years. Its population increased from 700,243 in 2015 to 772,268 in 2019, a notable 10.3% growth rate. This increase far exceeded both state and national averages during the same period, underscoring the county's growing appeal as a residential and economic hub. The rapid growth is attributed to factors such as its coastal location, economic opportunities, and a steady influx of retirees and families attracted to its quality of life and natural amenities. This demographic expansion has placed Lee County among Florida's fastest-growing regions, highlighting its increasing importance within the state. Figure 2.1 maps mangrove extent in Lee County using Global Mangrove Watch (GMW) data for 2017 (Bunting et al. 2022), overlaid with the locations of single-family home sales from 2015 to 2019. Lee County contains a substantial stretch of coastal mangroves, with residential properties located both near and far from these natural features. Notably, some homes are oriented such that both mangroves and open water (ocean or bay) lie in the same direction, while for others, they lie in opposite directions. This spatial variation provides a unique setting to examine the role of mangrove protection in influencing property values, as illustrated later in Figure 2.3 and Figure 2.4.

2.3 Empirical Strategy

Mangrove protection proxy

To represent the protective role of mangroves in coastal housing markets, our study constructs a protection proxy that integrates both proximity and directional orientation of mangroves and the ocean relative to each property. This approach is grounded in extensive biophysical and ecological literature demonstrating that mangrove forests function as natural buffers against storm surge, wave energy, and coastal inundation, particularly when positioned between vulnerable assets and

storm surge. Our analysis does not incorporate wind and wave directions explicitly; instead, it focuses on the directional orientation of the ocean and mangroves relative to each property. Alongi (2008) emphasizes that the degree of protection offered by mangroves depends not only on forest structure and species composition but also on the angle of impact, highlighting how directional placement shapes the magnitude of buffering. Temmerman et al. (2023) further stress that mangroves are most effective in attenuating wind waves when vegetation stands in the path of the incoming storm. Their ability to attenuate storm surge is dependent on landscape features such as forest width, continuity, and the presence of tidal channels. In addition, Maza et al. (2017) demonstrate through flume experiments that flow velocity and turbulence are highest at the leading edge of a mangrove forest and diminish progressively into the interior. Trees situated directly in the path of flow bear the greatest drag, suggesting that only mangroves located in front of a property, relative to incoming waves or surge direction, can reduce hydrodynamic forces. The findings from Alongi (2008), Maza et al. (2017) and Temmerman et al. (2023) and the broader literature collectively indicate that spatial configuration, specifically proximity and directional positioning plays a central role in determining the effectiveness of mangrove ecosystems in providing protection.

Figure 2.2 illustrates the limitations of traditional proximity-based measures in defining mangrove protection. In such measures, all properties located near mangroves are uniformly classified as protected, regardless of whether the mangroves lie seaward or landward of the structures. This approach leads to misclassification, particularly in coastal settings where properties may be closer to mangroves on the bay side while remaining directly exposed to the ocean. In the map, the protection dummy is defined solely based on proximity to mangroves. Yellow dots represent houses perceived as protected because they are relatively closer to

mangroves than to the ocean, while red areas are not considered protected based on this distance metric alone. However, some properties classified as protected under this approach remain vulnerable because their geographic location leaves them exposed to the ocean or bay despite nearby mangroves. This misalignment illustrates the importance of incorporating directional shielding in defining protection. To address this limitation, we introduce directional-proximity-based proxy.

The directional-proximity-based proxy identifies as protected only those properties that are both near mangroves and have mangroves positioned between the property and the ocean. The conceptual framework for this proxy is illustrated in Figure 2.3. It depicts two scenarios, in the first - the house is located on the seaward side of the mangroves, leaving it unprotected from high waves, in the second - mangroves are positioned between the ocean and the house, acting as a natural barrier against wave impacts. This spatial relationship forms the basis for our definition of the *Protected* variable, capturing the mitigating role of mangroves in safeguarding properties from storm surge.

We use the county's coastal boundary to map the shoreline and Global Mangrove Watch (GMW) data (Bunting et al., 2022), from 2015 to 2019 to map mangrove extents. For each property, we calculate the distance and angle to both the nearest mangrove extent and the nearest shoreline. To assess directional protection, we compute the angular difference between the mangrove and shoreline directions relative to each property. To account for edge cases where angular measurements cross the -180° to 180° boundary, we apply wraparound adjustments to ensure that the true directional relationship is captured. The next step involves determining directional alignment. To determine whether mangroves and the shoreline lie in the same direction relative to a property, we calculated the angular difference between their respective bearings from

each property and applied a threshold angle. We evaluated a range of thresholds (45° to 120°) to determine a cutoff beyond which the two features could no longer be considered directionally aligned. Based on this, we adopt a 90° threshold which means if the angular difference between the mangrove and shoreline bearings is less than 90°, the two are considered directionally aligned relative to the property. We then combine this directional alignment variable with a *closer_to_mangroves* dummy, which equals one if the property is located closer to mangroves than to the shoreline. The product of these two dummies defines the *protected* variable, identifying properties that are both nearer to mangroves and directionally positioned to plausibly benefit from their protective function. Detailed examples illustrating this process are provided in the Appendix. The GIS-based implementation of this method is illustrated in Figure 2.4. The variables are formally defined as:

where:

$$closer_to_mangroves = \begin{cases} 1, if \ dist_{mangrove} < \ dist_{ocean} \\ 0, \ otherwise. \end{cases}$$

and,

$$same_direction = \begin{cases} 1, if \ angle \ difference < 90^{\circ} \\ 0, \quad otherwise. \end{cases}$$

By incorporating both proximity and directional alignment, the mangrove protection proxy offers a more ecologically valid and policy-relevant measure of natural coastal defense, consistent with empirical insights from studies such as Alongi (2008), Chen et al. (2021), Maza et al. (2017)

and <u>Temmerman et al. (2023)</u>. This refinement captures a more nuanced nature of coastal protection that arises from the spatial orientation of mangroves relative to the ocean.

Econometric specification

This paper leverages the landfall of Hurricane Irma in Florida as a quasi-experimental shock to estimate the protective services provided by mangroves, as reflected in housing market capitalization. Hurricane Irma struck as a Category 4 storm in September 2017 and was one of the most damaging hurricanes in U.S. history, with estimated economic losses exceeding \$50 billion (Narayan et al., 2019). It made landfall in Florida, causing extensive flooding and storm surges of up to ten feet, particularly along the mangrove-dominated coastlines of the Everglades National Park. As one of the costliest hurricane years on record, 2017 brought attention to the role of natural coastal features in mitigating flood damage, offering a salient context to assess whether mangroverelated protection is capitalized in property values. Our study employs the hedonic property pricing model to analyse the impact of mangroves on property values within the coastal buffer of Lee County, focusing on a comparative assessment before and after Hurricane Irma. Our methodology hinges on using property sales prices as the dependent variable, with structural and environmental characteristics, alongside the hurricane event, as independent variables. We exclude island scenarios from our analysis. These include properties that are surrounded by the ocean, by mangroves, or by both. Since our interest is coastal single-family property, we create a binary buffer of 1-kilometer (K) as indicated in Figure 2.5, to identify the properties located within a 1K distance from either mangroves' extent or ocean boundaries. We further perform a robustness check using a 2K buffer.

We employ a DID approach to examine how protection by mangroves affected house prices after the hurricane. To support the identifying assumption of the DID framework, that the level of

mangrove protection remained relatively stable across treatment and control units over time—we compare mangrove extent before and after Hurricane Irma using GMW maps for 2016 and 2018 as shown in Figure 2.6. GMW Version 3.0 delivers annual mangrove extent maps for 1996, 2007– 2010, and 2015–2020 with each map independently derived from satellite data of that year. This ensures that our comparisons across the years are grounded in independently derived observations. Our study area, located north of the most severely affected zones, shows no visible large-scale changes in mangrove coverage between these two years. While the mapped extent appears stable, the literature emphasizes that mangrove protection is not static; storm-related damage and subsequent recovery can significantly influence the functional capacity of these ecosystems. Most severe mangrove damage occurred farther south, at the southern tip of Florida, particularly in the Everglades and in Monroe and Collier counties (Lagomasino et al., 2021). Nonetheless, the absence of visible extent loss in our study region, combined with evidence of early regeneration and functional recovery in mangrove systems (Temmerman et al., 2023), lends support to the assumption that protection levels remained relatively stable during the post-Irma period analyzed. Following the standard hedonic property price model, the sale price of a property is expressed as a function of its structural attributes, locational characteristics, and environmental amenities. Structural attributes include the number of bedrooms and bathrooms, total living area, presence of a garage or pool, and other property-specific features. Locational characteristics reflect proximity to services such as supermarkets, healthcare facilities, parks, schools, and the coastline. Environmental amenities refer to natural features that may enhance or reduce the desirability of a location.

To isolate the causal impact of mangrove protection on property values, the main analysis employs a repeat sales model with property fixed effects. This approach controls for all time-

invariant, unobserved characteristics at the property level such as structural features that could otherwise bias estimates in a standard hedonic regression. The estimation is restricted to properties that were sold both before and after Hurricane Irma, allowing for a within-property comparison of price changes over time. Our analysis assumes that no major gray infrastructure investments confound the observed post-Irma price changes. Based on available information, there is no indication that flood defense structures were constructed in Lee County during the immediate aftermath of Hurricane Irma within the years covered in our dataset.

Equation (1) models the logarithm of the sale price (P_{it}) as a function of perceived mangrove protection $(Protected_i)$, the hurricane event indicator $(Hurricane_t)$, and their interaction, while controlling for property fixed effects (α_i) and quarter-year (λ_t) fixed effects. Protected is a binary variable equal to one if the property is considered protected by mangroves, based on its spatial orientation relative to the ocean. $Hurricane_t$ is an event dummy that indicates sales transactions occurring after September 10, 2017.

The model is specified as follows:

$$\ln(P_{it}) = \beta_m Protected_i + \beta_h Hurricane_t + \beta_e (Protected_i * Hurricane_t) + (1)$$

$$\alpha_i + \lambda_t + \varepsilon_{it}$$

In equation (1), the interaction term between *Protected* and *Hurricane* is our variable of interest; it captures the differential change in property values for homes considered protected by mangroves, relative to unprotected homes, after the hurricane. The quarter-year fixed effects account for market-wide shocks affecting all properties within a given quarter.

We also run a Census block fixed effects (γ_n) model with quarter-year fixed effects (λ_t) using the following specification:

$$\ln(P_{it}) = \beta_0 + \beta_x \ X_i + \beta_m Protected_i + \beta_h \ Hurricane_t$$

$$+ \beta_e \ (Protected_i * Hurricane_t) + \alpha_i + \lambda_t + \varepsilon_{it}$$
(2)

Equation (2) complements the property fixed effects model by capturing variations within Census blocks, allowing us to examine how a property's structural characteristics, its location relative to points of interest, and its position within the floodplain collectively influence property prices. Building on the framework of (Atreya & Ferreira, 2015), we initially incorporated a *Damage* proxy and used water depth from flood insurance claims obtained through the National Flood Insurance Program (NFIP) website, which reports water depth at the individual claim level. However, this approach was ultimately not used in the final analysis due to limitations discussed later in the paper.

2.4 Data & Descriptive Statistics

The study utilizes sales records of single-family residential homes in Lee County, Southwest Florida, from 2015 to 2019. While this represents a relatively short timeframe, it reflects the most recent four years of available transaction data as of October 2022, and it covers a symmetric window of property transactions before and after Hurricane Irma in September 2017. Property sales data are drawn from the Lee County Property Appraiser database, which includes structural characteristics like lot size, square footage, year built, and presence of amenities such as a pool, garage, or seawall. The seawall variable indicates whether a property adjacent to a water body has a hardened coastal defense structure, which may affect both its market value and perceived

resilience to flooding. However, the dataset does not include information on the timing of seawall installation, so the variable is treated as time-invariant in our analysis.

The dataset is spatially enriched by linking each property to environmental and locational features, including distance and directional proximity to mangroves, flood risk zones, and proximity to points of interest such as schools, hospitals, supermarkets, and recreational centers. GMW data are used to compute the distance and angle from each house to the nearest mangrove patch. We also calculate each property's angle and distance to the open coastline using county shoreline data. A mangrove protection proxy is constructed based on whether mangroves lie between the house and the coast, capturing the potential role of mangroves in attenuating storm surge. Flood zone classifications come from FEMA's Flood Insurance Rate Maps and elevation data derived from digital elevation models. We also use TIGER/Line shapefiles to assign each parcel to its respective census block, tract, and ZIP code, enabling controls for neighbourhoodlevel fixed effects. Finally, we incorporate flood insurance data from the National Flood Insurance Program (NFIP), which provides water depth at the census block group. Given the inclusion of property fixed effects in equation (1), these aggregated measures do not provide any temporal variation and are not used in this specification, but they are used in the census block specification in equation (2).

Sale prices are adjusted to 2019 dollars using Lee County housing price index data from the Federal Reserve Economic Data (FRED). The literature does not provide standardized guidance on handling multiple transactions for the same property within short time frames. To minimize the risk of including non-arm's length sales, transactions where the same property was bought and sold multiple times within a few months were excluded. After cleaning and filtering, the dataset contains 100,794 unique transactions. We further restrict the analysis to properties located within

a 1 K buffer of either the mangrove edge or the shoreline, yielding a final estimation sample of 19,234 transactions. Properties located on barrier islands are excluded, as they represent a distinct housing submarket with systematically higher prices and limited comparability to mainland parcels.

Among the 19,234 sales transactions within the 1-kilometer buffer, 10,543 occurred before Hurricane Irma and 8,691 occurred after. We construct a repeat sales panel by identifying properties that were sold in both periods surrounding the hurricane, which made landfall in September 2017. A total of 1,452 properties appears in both periods, of which 455 are perceived as protected. Retaining all transactions for these repeat-sale properties, including 1,636 pre-Irma sales and 1,536 post-Irma sales, results in a panel of 3,172 repeat-sale observations. Table 2.1 presents the distribution of sales transactions before and after Hurricane Irma, disaggregated by whether properties are protected by mangroves or not. Since directional alignment is largely time-invariant, the protection status of each property is assumed to remain unchanged over time. The table includes both the full set of transactions within the 1-kilometer buffer and the subset of repeat sales.

A limitation of the repeat sales design is the reduction in sample size, as it includes only properties that transacted in both the pre- and post-hurricane periods. Nonetheless, the summary statistics reported in Table 2.2 indicate that properties in the repeat sales sample are broadly like those in the full estimation sample in terms of structural characteristics, location, and exposure to environmental risks. Two-sample t-tests reveal that repeat sales properties tend to have slightly lower prices, smaller total area, and are situated at marginally lower elevations. Differences in environmental features, including distance to mangroves and inundation depth, are not statistically significant. Core structural features, such as the number of bedrooms and stories, show no

differences. Overall, while the repeat sales sample modestly underrepresents higher-value homes, it remains broadly representative of the larger sample, supporting its use in analyzing price dynamics over time. This suggests that selection into the repeat sales sample does not disproportionately capture properties with higher storm vulnerability during the relatively short pre- and post-hurricane period analyzed.

2.5 Results

Table 2.3 presents an estimate from a repeat sales property fixed effects model examining the relationship between mangrove protection and housing prices within a 1-kilometer buffer. Two model specifications are reported: Model 1 defines protection using the directionality-based approach put forth in this paper (closer to mangroves × same direction); Model 2 defines protection more simply, based solely on the property's proximity to mangroves (closer to mangroves). In both models, property fixed effects absorb all time-invariant unobserved heterogeneity and standard errors are clustered at the property level since census blocks are comprised of both protected and not protected housing units. Across both specifications, the coefficient on the Protected indicator is positive but not statistically significant. The hurricane indicator is positive and statistically significant in both the models, suggesting an overall increase in property prices following Hurricane Irma, likely driven by post-disaster recovery dynamics. Substantial federal assistance, including FEMA redevelopment funding and insurance payouts, contributed to rebuilding efforts and may have supported property values during the post-Irma period (Federal Emergency Management Agency (FEMA), 2018). The interaction between the Protected and Hurricane indicators is positive and statistically significant at the 10% level in both models.

The results show that the directionality-based measure of mangrove protection (Model 1) yields a larger interaction effect between protection and hurricane exposure. Properties classified as protected under this definition experienced approximately an 8.0% price premium following the hurricane. In contrast, the simpler proximity-based measure (Model 2) also shows a statistically significant interaction effect, but the estimated premium is approximately 6.1%. These results suggest that incorporating the directional relationship between mangroves, properties, and the ocean captures variation in protective value that may be missed by distance-based definitions alone.

We also re-estimate the above regressions using year fixed effects, with results reported in Table 2.7 of Appendix A. In model 1a, the interaction term based on the directionality-based protection measure remains statistically significant, showing a 7.6% price premium post-hurricane periods, reinforcing the robustness of this approach. In contrast, model 2a, which defines protection solely based on proximity to mangroves, yields an insignificant interaction term, suggesting limited explanatory power when relying on distance alone.

To validate the identifying assumption of parallel trends underlying our DID framework, we conduct a basic comparison of pre- Irma prices. A two-sample t-test comparing pre-Irma adjusted log prices between protected and unprotected properties yields a t-statistic of -8.02 and a p-value below 0.01. The difference in mean log prices is statistically significant at the 1% level, with a 95% confidence interval ranging from -0.460 to -0.279. These results indicate that protected properties were priced significantly higher than unprotected properties. Next, we test parallel trends assumption using an event study approach, with 2017 as the base year. This specification allows us to trace the evolution of treatment effects before and after the event, relative to the base year. The pre-treatment coefficients for 2015 and 2016 are small in magnitude and statistically

insignificant. A Wald test of joint significance for the 2015 and 2016 interaction terms yields a chi-squared statistic of 1.14 with a p-value of 0.32, providing additional support for the parallel trend assumption. Figure 2.7 plots the event study coefficients and their 95% confidence intervals for both the annual and quarterly specifications, using 2017 and 2017 Q3 as the base periods, respectively. In the annual event study, estimates remain close to zero in the pre-event years, followed by an upward shift in 2018, indicating a positive price effect of protection in the post-treatment period. In the quarterly specification, pre-treatment coefficients are close to zero and statistically insignificant, except for 2017 Q1 and somewhat Q2. A positive and statistically significant effect appears in 2017 Q4, while estimates for subsequent quarters are small in magnitude and not statistically significant. The lack of statistically significant effects in subsequent quarters may reflect greater noise at the quarterly level. Finally, Figure 2.8 presents average adjusted prices across quarter-years for protected and unprotected properties. Prior to Hurricane Irma, price trends for both groups move in parallel, although protected properties exhibit slightly higher price levels.

To ensure the reliability of our estimates, we perform a series of robustness and falsification tests. First, we expand the spatial scope of the analysis to include properties located within a 2 K buffer of either the mangrove edge or the coastline. This broader window accounts for properties that may still benefit from mangrove protection or be vulnerable to coastal hazards but lie slightly beyond the original spatial threshold. Table 2.4 presents the results. The interaction term between *Protected* and *Hurricane* remains positive and statistically significant, with an estimated coefficient of 0.0938, suggesting a 9.4% price premium for protected properties in the aftermath of a hurricane. The larger price effects observed when we include more inland properties are consistent with broader post-disaster market dynamics in Florida.

As a falsification test, we conduct a placebo analysis using alternative event dates, including dates both before and after the actual event as presented in Table 2.5. Specifically, we replace the actual hurricane date (September 10, 2017) with placebo dates - September 10, 2016, and September 10, 2018 - in separate tests. The estimated interaction between *Protected* and the placebo hurricane indicator is statistically insignificant in both scenarios, lending support to the validity of our identification strategy. The absence of an effect in this falsification exercise reinforces the interpretation that the main results are not driven by underlying trends or spurious correlations.

We next estimate a hedonic regression with census block fixed effects, using the full sample of properties within the 1K buffer. Results for the key variables—protection, hurricane, and their interaction—are presented in Table 2.6. In this specification, the interaction between the protection dummy and the hurricane indicator is negative and statistically significant, in contrast to the results from the property fixed effects model. However, given the larger number of observations in the pooled regression, these differences might be driven by sample composition rather than model structure alone. The full regression output, including all housing characteristics and environmental controls, is provided in Appendix Table 2.8. Across these specifications, we observe expected signs for most housing characteristics. Structural attributes such as additional bathrooms, garages, and seawalls are positively associated with sale prices, while older homes and homes with additional stories tend to sell at a discount. Elevation is positively associated with price, and proximity to the coastline is also valued more highly, even after controlling flood zone status. Amenities such as proximity to recreational centers and healthcare facilities do not show significant effects, whereas proximity to county parks is positively associated with property values.

When fixed effects are specified at the neighbourhood level (census block), much of the variation in perceived protection may be absorbed, leading to an attenuation of the estimated price premium. This divergence suggests that the protective value of mangroves operates at a more localized, property-specific level rather than uniformly across neighbourhood. It also reinforces the motivation behind our construction of a protection proxy that incorporates the relative directionality of mangroves and the ocean for each property. Finally, the pooled regression results show that key housing and locational attributes exhibit expected relationships with prices, lending further confidence to the overall specification and control structure.

2.6 Discussion

The empirical results provide evidence that mangroves play a measurable and economically important role in protecting residential properties from hurricane related risks. Although flood resilience planning and funding allocations were initiated in the years following Hurricane Irma (Flooding Facts, 2024; Flooding Information - Irma), there is no indication of significant flood protection infrastructure being constructed in Lee County during the immediate aftermath of the hurricane within our study period and within our study area, especially for homes located within 1 km or 2 km of the coastline or the nearest mangrove fringe. In the repeat sales framework, which controls for time-invariant unobserved property characteristics, we find that properties identified as protected by mangroves experienced significantly higher price appreciation following Hurricane Irma of about 8 percent. The robustness of the interaction effect in the expanded 2K buffer further supports this interpretation, suggesting that the valuation of mangrove protection is not confined to narrowly defined coastal segments but may extend inland to properties that still perceive benefits from nearby natural buffers.

Additional analyses further reinforce the robustness of these findings. Placebo tests using alternative event dates yield no significant effects, lending credibility to the causal interpretation of the main results. Event study estimates confirm parallel pre-trends between protected and unprotected properties, consistent with the identifying assumptions of the difference-in-differences framework. While the quarterly event study exhibits greater noise and smaller post-treatment effects beyond the immediate aftermath of the hurricane, this is expected given smaller sample sizes per period. At the same time, results from the full hedonic models with census block fixed effects reveal more complex dynamics. While key housing attributes such as structure size, elevation, and proximity to the coast continue to exhibit expected signs and significance levels, the estimated interaction between protection and hurricane becomes attenuated or statistically insignificant in these specifications. This likely reflects the limitations of neighbourhood level fixed effects in capturing the nuanced, property-specific ways in which natural protection is perceived and valued. Much of the variation in perceived protection is likely absorbed when fixed effects are defined at broader spatial units, thereby muting localized dynamics. These findings highlight the importance of constructing a refined protection proxy that accounts for the relative directionality between mangroves, the ocean, and individual properties, acknowledging that the protective function of mangroves is perceived differently at a finer spatial scale.

Overall, the findings underscore that the protective value of mangroves is recognized and capitalized into housing prices, particularly following major storm events, and that perceived protection is localized and property-specific rather than uniformly distributed across the neighbourhood.

2.7 Conclusion

This paper examines whether the protective presence of mangroves is recognized in property markets, particularly during extreme weather events. Using a repeat sales framework and property-level data, we find that homes identified as protected by mangroves experienced a noticeable increase in price appreciation following Hurricane Irma and remain stable when extending the spatial buffer to include properties up to 2K from the coast. This suggests that the market does not just value proximity to mangroves but also perceives their presence in reducing exposure to storm surge. Our approach goes beyond standard proximity-based measures by accounting for the relative direction of mangroves and the shoreline, which allows for a more spatially explicit assessment of protection.

These findings contribute to a growing body of literature on the economic valuation of ecosystem services, particularly those related to natural infrastructure and climate adaptation. By quantifying the protective effect of mangroves on housing prices, this study supports a nature-based approach to resilience. Mangroves offer a cost-effective alternative to hard infrastructure in flood mitigation, and their value is being capitalized in real estate markets. These results offer practical insights for policymakers and coastal planners. As climate change intensifies hurricane and flood risks, integrating natural infrastructure into economic and policy planning is no longer just about conservation, it is also a smart financial and risk management strategy for the future.

Table 2.1: Spatial and Temporal Distribution of Sales Transactions (2015-2019) within 1K buffer

	All transactions		Repeat sales	
	Pre Irma	Post Irma	Pre Irma	Post Irma
Not Protected	7401	5926	1125	1063
Protected	3142	2765	511	473
Total	10543	8691	1636	1536

Table 2.2: Summary Statistics for within 1K buffer and for repeat sales houses

	All transac	ctions	Repeat sal	es		
Variables	Mean	Std. dev	Mean	Std. dev	t stats	p-value
Sales Price (\$1000)	434.73	454.58	397.61	364.43	3.8244	0.0001
Total Area (sq ft)	3769.18	1832.82	3686.28	1684.96	2.5345	0.0113
Bedrooms	3.01	0.70	3.02	0.70	-1.2200	0.2225
Bathrooms	2.31	0.77	2.28	0.72	2.2183	0.0266
Garage	0.84	0.36	0.84	0.36	-	-
Carport	0.09	0.30	0.10	0.30	-	-
Pool	0.56	0.50	0.56	0.49	-	-
Boat dock	0.18	0.38	0.17	0.37	-	-
Seawall	0.26	0.44	0.25	0.43	-	-
Stories	1.13	0.34	1.13	0.33	1.0423	0.2973
Age	28.99	20.15	31.05	20.86	-5.1919	0.0000
Elevation (ft)	2.38	1.01	2.33	0.96	2.7052	0.0069
Distance to school (ft)	7020.52	4825.74	6987.91	4765.30	0.3564	0.7216
Distance to healthcare (ft)	7134.60	3683.36	7152.06	3624.68	-0.2509	0.8019
Distance to Supermarket (ft)	6006.00	4396.80	6001.01	4401.80	0.0591	0.9529
Distance to Recreation centre (ft)	2897.90	1707.70	2852.09	1681.71	1.4183	0.1562
Distance to Park (ft)	9029.26	6392.40	9061.38	6462.16	-0.2598	0.7950
Distance to mangroves (ft)	6565.82	5826.60	6748.31	5764.60	-1.6494	0.0991
Distance to coastline (ft)	2369.60	1822.53	2323.10	1769.83	1.3650	0.1723
Inundation depth (inches)	1.04	2.03	0.98	1.88	1.8518	0.0641
Flood Zone	0.74	0.44	0.74	0.44		
Protected	0.31	0.46	0.31	0.46		

Table 2.3: Property Fixed Effects Regression Output within 1K

	Model 1	Model 2
	(Directionality)	(Proximity)
Variables	Log(price)	Log(price)
Protected (=1)	0.3093	0.0279
11000000 (1)	(0.2682)	(0.1378)
Hurricane (=1)	0.2817	0.2697
Trufficanc (-1)	(0.1449)	(0.1445)
Protected x Hurricane	0.0799*	0.0614*
Frotected x Trufficane	(0.0313)	(0.0305)
Fixed-Effects:		
Quarter-year	Yes	Yes
Property	Yes	Yes
S.E.: Clustered	Property	Property
Observations:	3,172	3,172
R2	0.85153	0.85106
37 1 1	1 alcalcala	0.01 shale 0.07 sh 0.1

Note: standard errors in parentheses; ***p < 0.01, **p<0.05, *p<0.1

Table 2.4: Robustness Check with Property Fixed Effects Regression Output within 2K

	Model 3
Variables	log(price)
Protected (=1) Hurricane (=1) Protected x Hurricane	0.1542 (0.1176) 0.4551*** (0.1112) 0.0988*** (0.0233)
Fixed-Effects:	
Quarter-year	Yes
Property	Yes
S.E.: Clustered	Property
Observations:	5,865
R2	0.84567

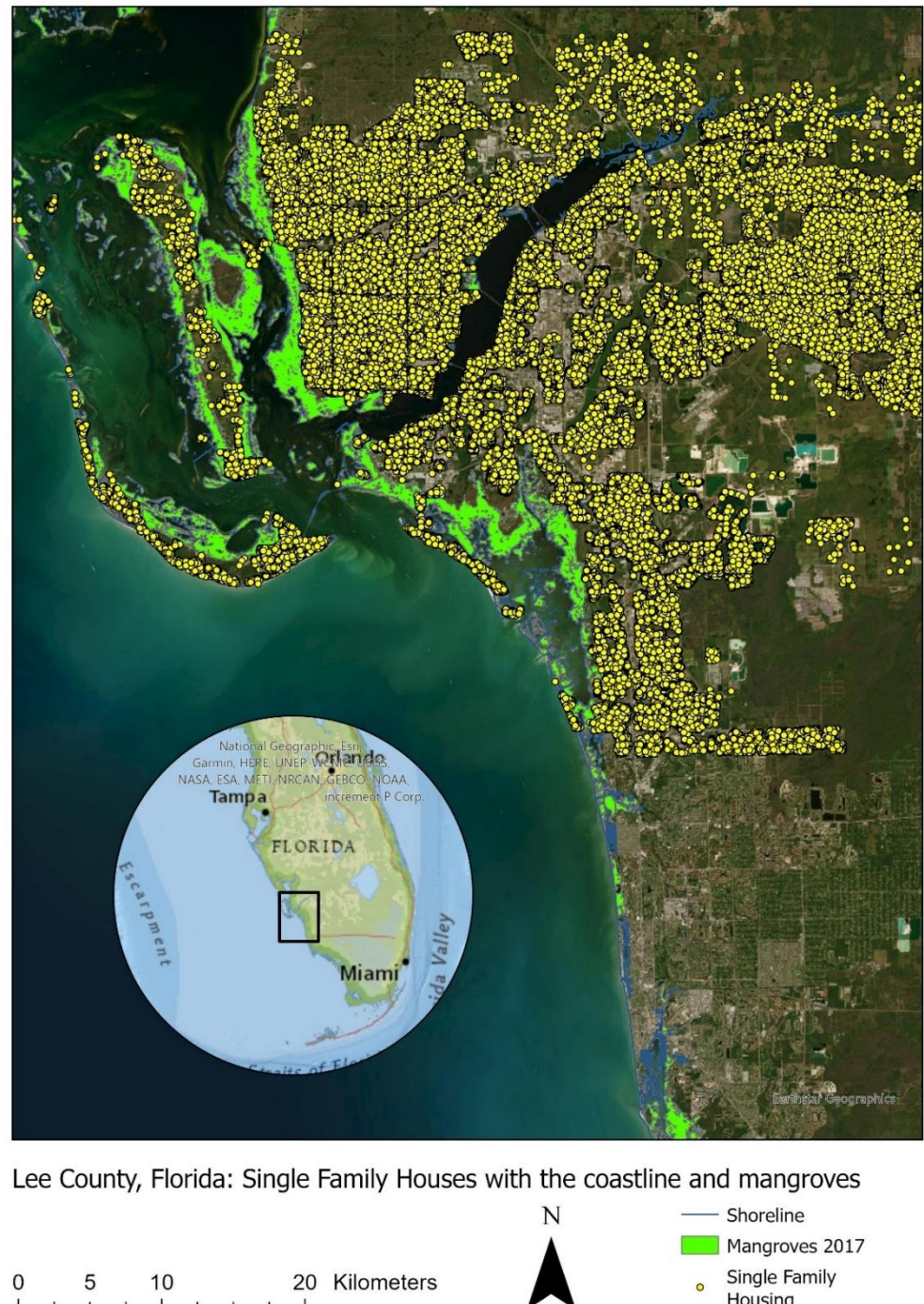
Table 2.5: Placebo Test

	Model 4	Model 5
	Before Hurricane	After Hurricane
Variables	log(price)	log(price)
Protected (=1)	0.2874 (0.2729)	0.3121 (0.2664)
Placebo Hurricane (=1)	-0.1229 (0.1496)	-0.1270 (0.0880)
Protected x Placebo	0.0465	0.0396
Hurricane	(0.0367)	(0.0351)
Fixed-Effects:		
Quarter-year	Yes	Yes
Property	Yes	Yes
S.E.: Clustered	Property	Property
Observations:	3,172	3,172
R2	0.85082	0.85079

Note: standard errors in parentheses; ***p < 0.01, **p<0.05, *p<0.1

Table 2.6: Neighbourhood Fixed Effects Regression Output within 1K buffer

-	Model 6
	(All within 1K)
Variables	log(price)
	0.0332
Protected (=1)	(0.0260)
	0.0634
Hurricane (=1)	(0.0352)
	-0.0571***
Protected X Hurricane	(0.0154)
Fixed-Effects:	
Quarter-year	Yes
Census Block level	Yes
S.E.: Clustered	Census block
Observations:	19,234
R2	0.75388



Single Family Housing

Figure 2.1: Lee County Single Family Sales from 2015 to 2019

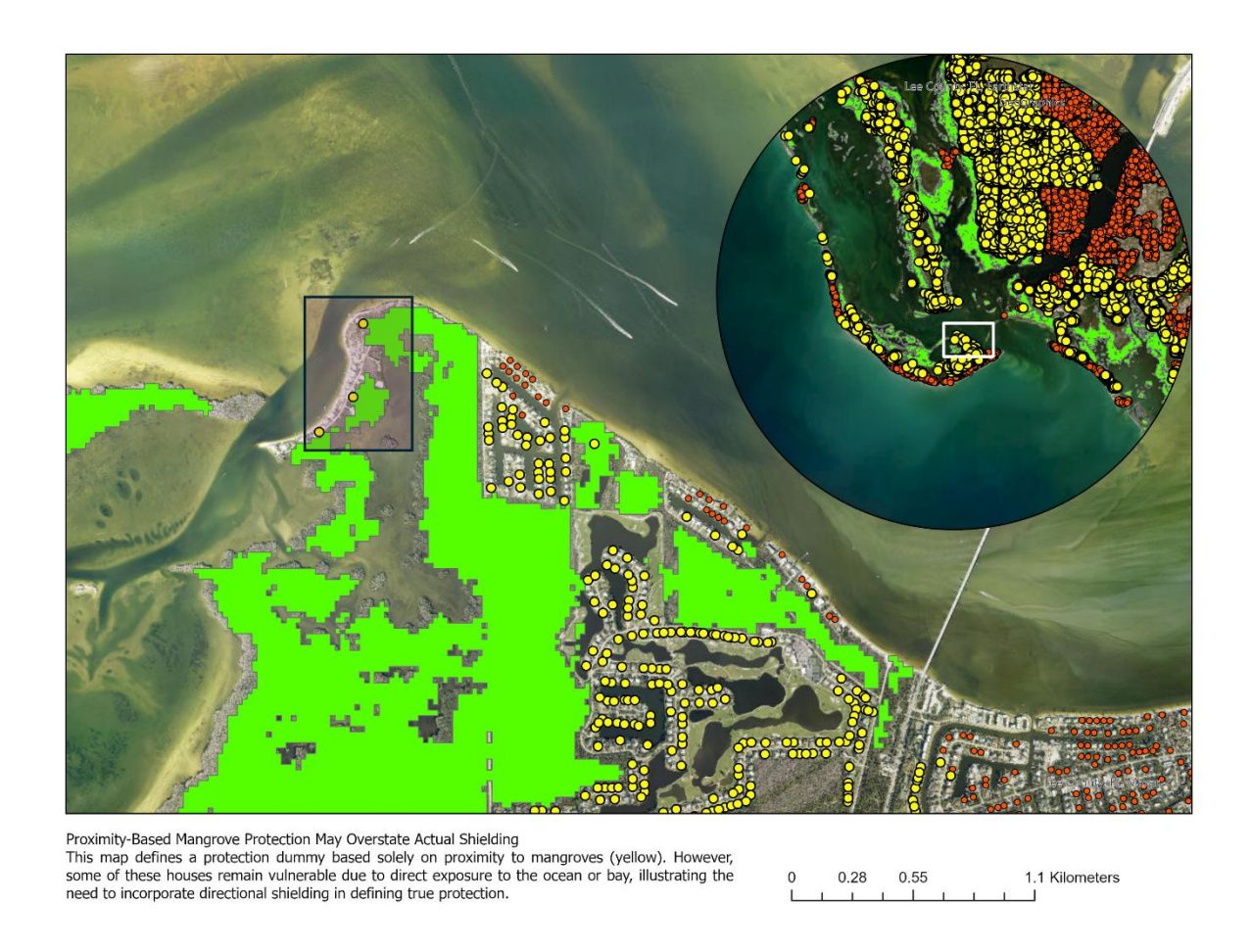


Figure 2.2: Proximity-based mangrove protection may overstate actual protection.

Note: This map defines the protection dummy based solely on proximity to mangroves. Properties shaded yellow are perceived as protected, while those in red are not. However, several properties (within the black rectangle) remain directly exposed to the ocean or bay despite their proximity to mangroves, illustrating that distance alone does not ensure actual protection. These spatial patterns underscore the importance of incorporating directional exposure to more accurately capture the protective role of mangroves.

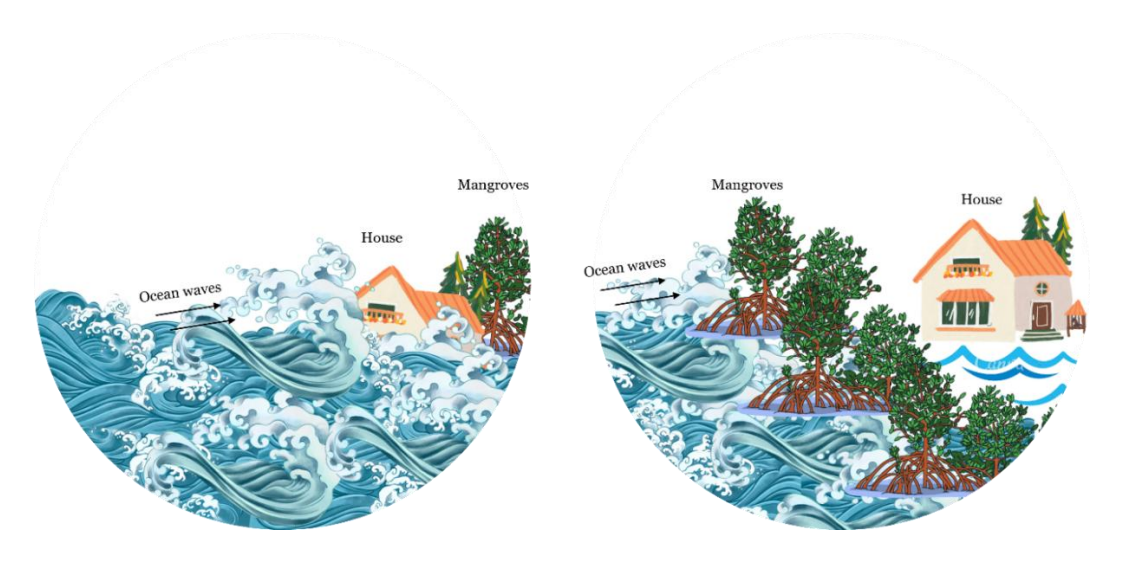


Figure 2.3: Determining protection status based on the relative positions of houses, mangroves, and the ocean.

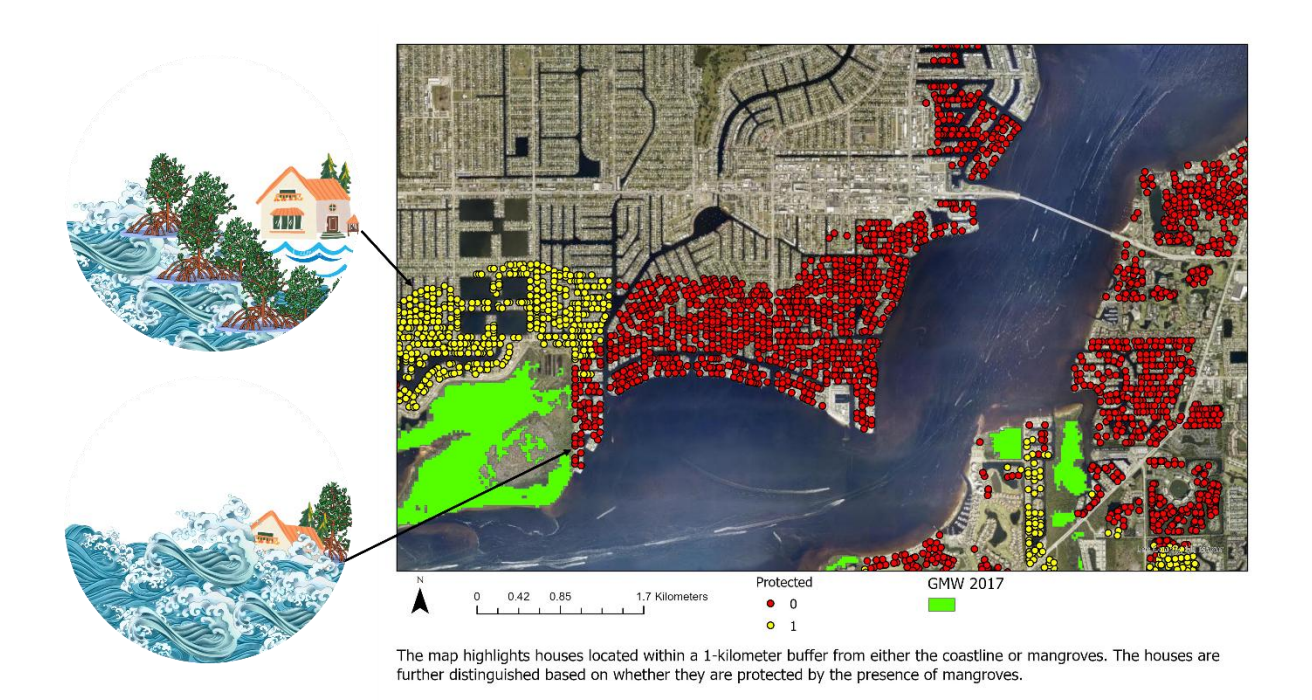
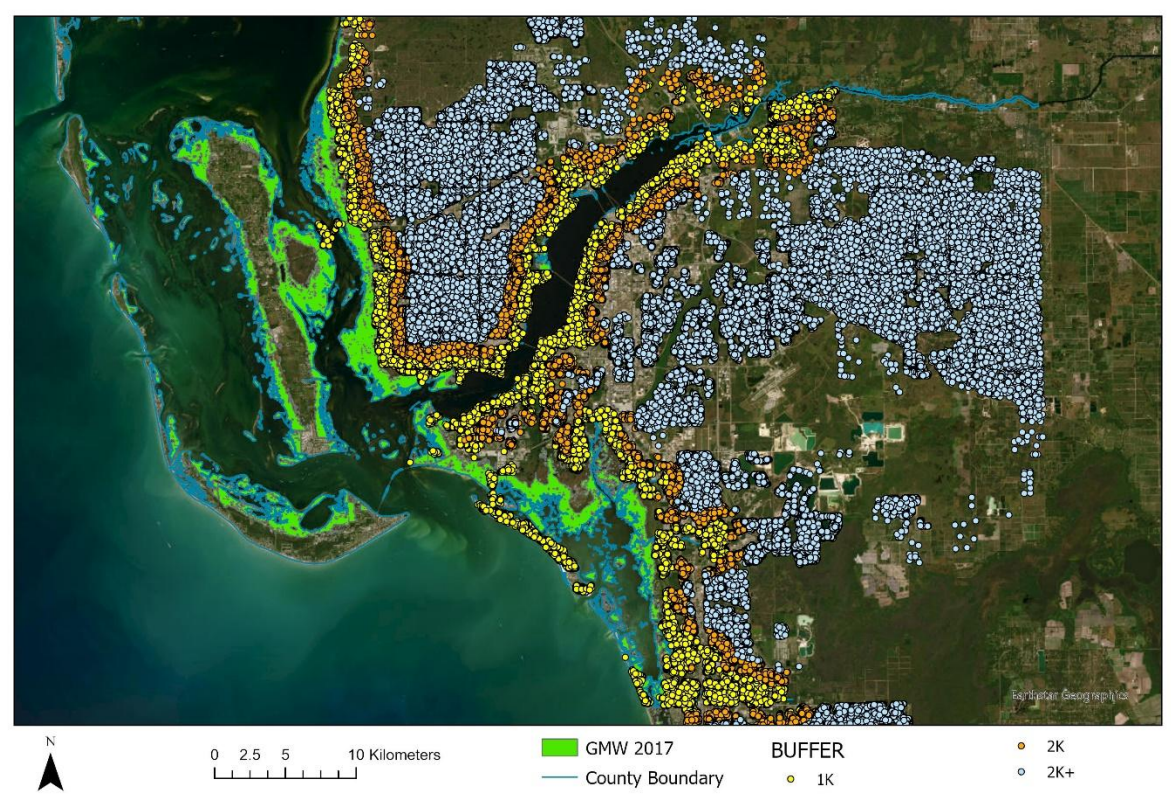


Figure 2.4: Directional Protection Concept and GIS-Based Implementation

Note: The left section illustrates conceptual scenarios demonstrating the importance of mangrove directionality in coastal protection: (i) a house positioned seaward of the mangroves remains exposed to storm impacts, whereas (ii) a house located landward is shielded from incoming waves. The right panel shows the application of this concept in ArcGIS Pro, where properties are classified as protected or unprotected based on their spatial relationship with nearby mangroves and the ocean. Some houses that appear visually behind mangroves are still shown as unprotected (red) rather than protected (yellow). This is due to the presence of small water inlets in the coastline shapefile. Our method defines protection based on the proximity and directional orientation of mangroves relative to the nearest coastline point. In areas with such inlets, this spatial configuration results in some houses being categorized as unprotected, even if they appear protected in the map view.



The map displays houses categorized by their proximity to mangroves and the coastline, divided into three buffer zones: within 1 kilometer, between 1 to 2 kilometers, and beyond 2 kilometers.

Figure 2.5: Spatial Distribution of Properties Relative to Coastal Features in Lee County

Note: We explicitly exclude island scenarios from our analysis. These include properties that are surrounded by the ocean, by mangroves, or by both.



Figure A. Mangrove Extent (2016)
Mangrove coverage from Global Mangrove Watch (GMW 2016) overlaid with single-family housing units. This map establishes pre-hurricane baseline conditions, illustrating mangrove distribution prior to Hurricane Irma

N

0 2.5 5 10 Kilometers GMW 2016

Single Family Houses

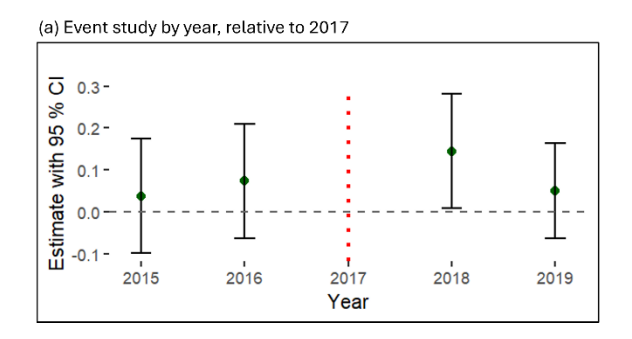


Figure B, Mangrove Extent (2018)
Post-hurricane mangrove extent from Global Mangrove Watch (GMW 2018), showing minimal observable change in coverage compared to 2016.

 N_z

Figure 2.6: Mangrove extent before and after Hurricane Irma.

Note: Panel A shows 2016 mangrove extent and Panel B shows 2018 extent, based on GMW maps. Yellow dots represent single-family homes within a 1 km buffer of mangroves or ocean.



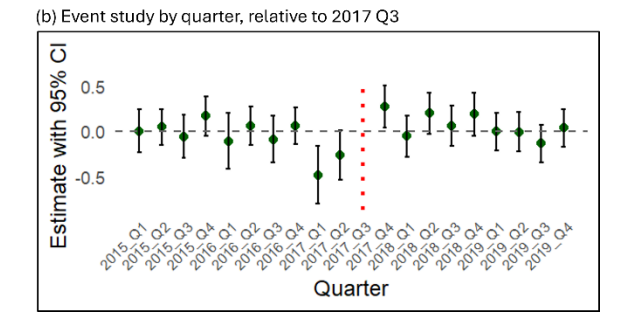


Figure 2.7: Event Study Plot

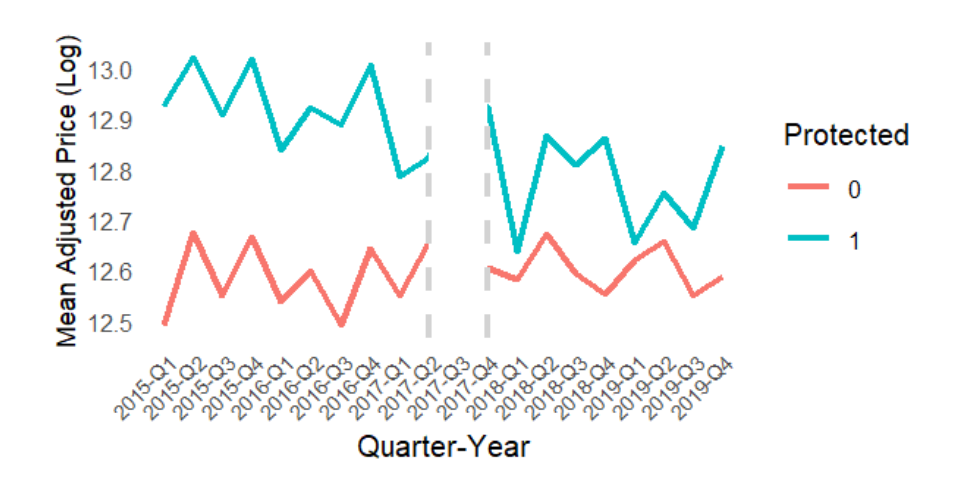


Figure 2.8: Pre-trend of the two group

Appendix A

The diagrams below illustrate scenarios to clarify the directional relationship between mangroves, the ocean, and a house, in a Cartesian coordinate system. The location of the house corresponds to the origin or point (0,0). These scenarios demonstrate how the angular difference and relative positioning of mangroves determine whether a house is considered protected. Each scenario includes a rough computation of the angular difference and the protection status.

Protection = same direction \times near mangroves

Scenario 1: Mangroves and ocean in the same direction, properties are protected (Figure 2.9).

The angular difference between the mangroves and the ocean is less than 90°, indicating alignment in the same direction. The mangroves are positioned between the house and the ocean, effectively acting as a protective barrier.

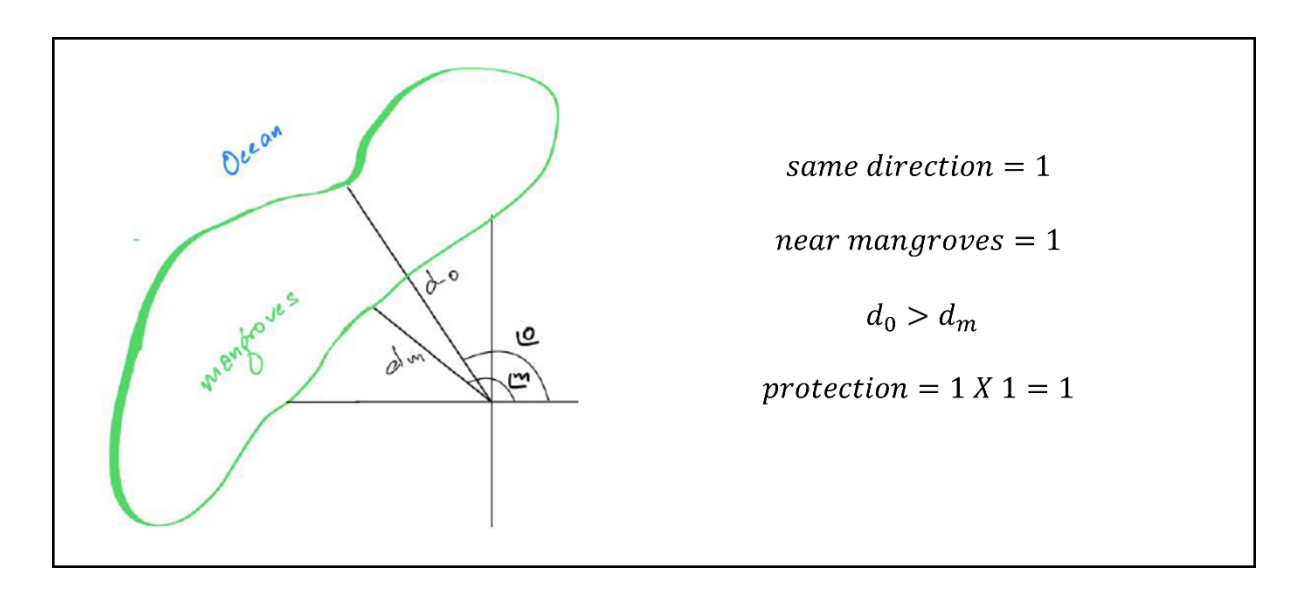


Figure 2.9: Mangroves & Ocean in the same direction, properties are protected

Scenario 2: Mangroves and Ocean in the same direction, properties are not protected (Figure 2.10). The angular difference between the mangroves and the ocean is less than 90°, indicating alignment in the same direction. However, the mangroves are not located between the house and the ocean, providing no effective protection. In this case, both same_direction and closer_to_mangroves dummies are 1, resulting in a protection value of 1.

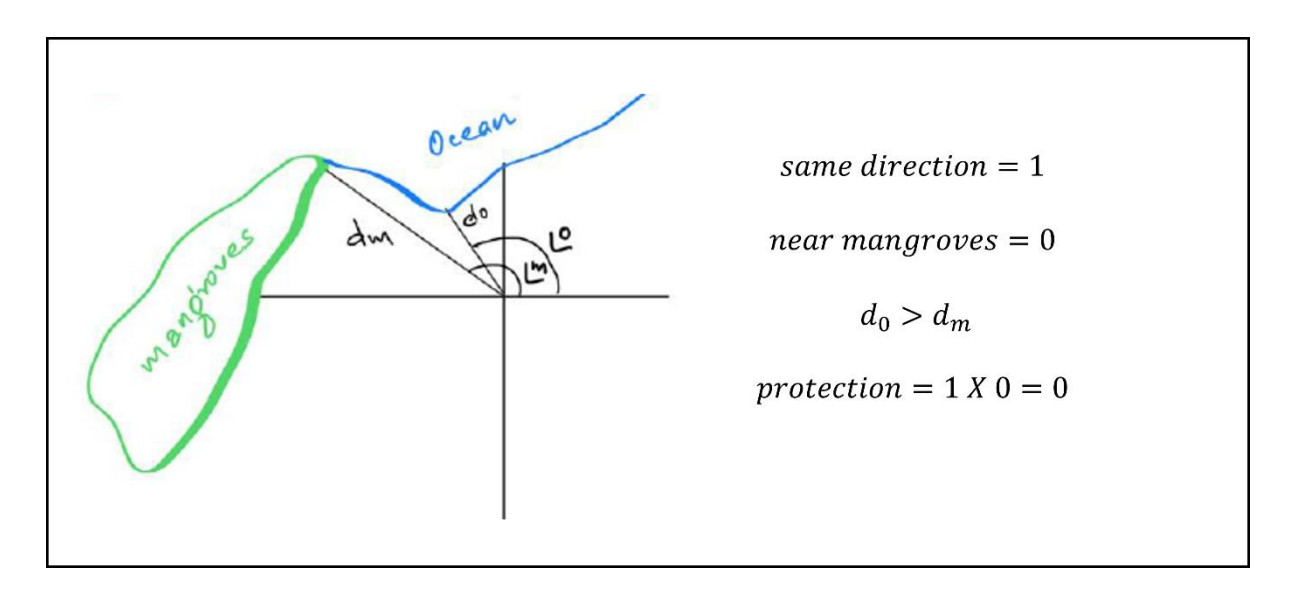


Figure 2.10: Mangroves & Ocean in the same direction, properties are not protected

Scenario 3 & 4: Mangroves and Ocean in the opposite direction, properties are not protected (Figure 2.11).

The angular difference between the mangroves and the ocean exceeds 90°, indicating they are not aligned. The house is considered unprotected because the directional alignment condition is not met. In this case, same_direction is 0, and protection is automatically 0, regardless of the closer_to_mangroves value.

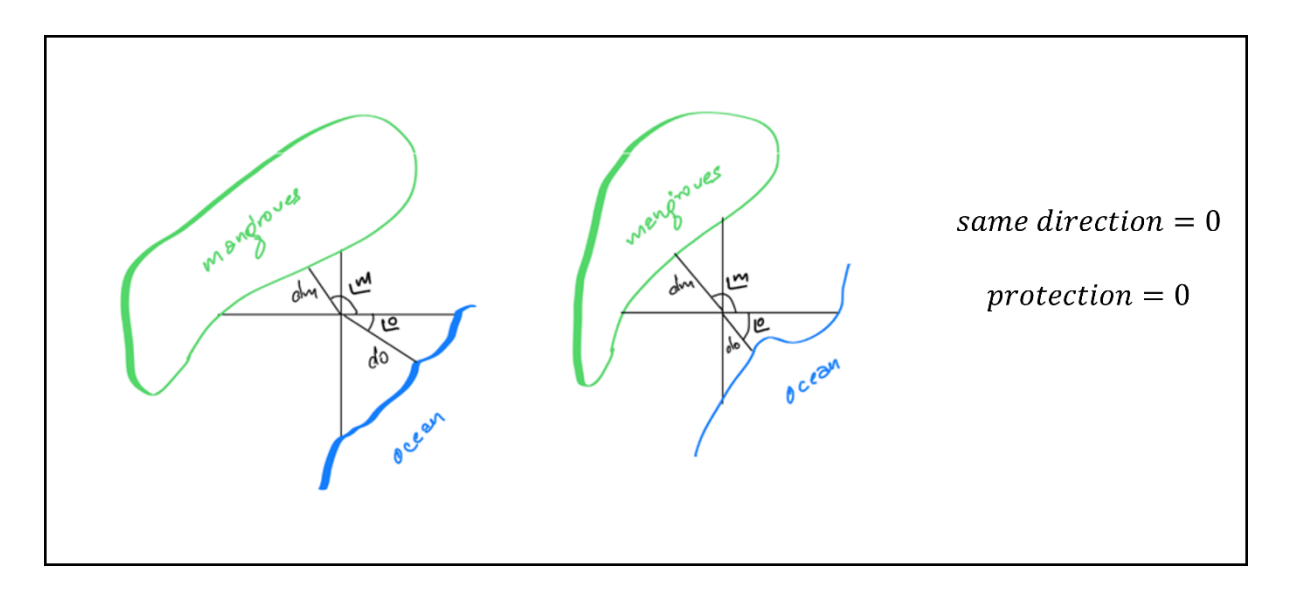


Figure 2.11: Mangroves & Ocean in opposite direction, properties are not protected

However, there is an edge case where the closer_to_mangroves dummy may require additional consideration. For instance, if the house is very close to the mangroves and the ocean is significantly farther away but in the opposite direction, the protection offered by mangroves may remain effective despite the lack of directional alignment. In such cases, the influence of the ocean's direction on protection might diminish, and the proximity of mangroves could take precedence. This scenario introduces complexity, and we are exploring how to integrate a proximity-based threshold for the closer_to_mangroves dummy to account for such cases. These edge cases will be addressed in further analyses and are critical for refining the computation of the protection variable.

In the scenarios above, to accurately represent the directional relationship between the nearest mangrove extent and the ocean, the angular difference is calculated as the absolute difference between their respective angles. However, in cases where this difference exceeds 180°, the value is adjusted to reflect the shortest rotational distance. This adjustment accounts for the wraparound

nature of angles measured in a circular system, ensuring consistency and correctness in the computation. The following examples illustrate this process:

- a. If the angle to nearest mangrove stretch is 20° and to the ocean is -40° then the angular distance is the absolute difference between then which is $abs(angle_{mangrove} angle_{ocean})$ which is $abs(20^{\circ} (-40^{\circ})) = 60^{\circ}$.
- b. Similarly, if the angle to nearest mangrove stretch is 100° and to the ocean is -100° then the absolute difference between them would initially be calculated as $abs(100^{\circ} (-100^{\circ})) = 200^{\circ}$. However, since 200° exceeds 180° , we adjust the same as $360^{\circ} 200^{\circ} = 160^{\circ}$. This adjustment ensures that the angular difference accurately represents the shortest rotational distance between the two directions.

Regression Output:

Table 2.7 presents result from alternative specifications. In Model 1a, the interaction term based on the directionality-based protection measure remains statistically significant, showing a 7.6% price premium post-hurricane periods, reinforcing the robustness of this approach. In contrast, model 2a, which defines protection solely based on proximity to mangroves, yields an insignificant interaction term, suggesting limited explanatory power when relying on distance alone.

Table 2.7: Alternative Protection Measure Based on Relative Proximity

Variables	Model 1a (Directionality) Log(price)	Model 2a (Proximity) Log(price)
Protected (=1)	0.2986 (0.2594)	-0.0140 (0.1462)

Hurricane (=1)	0.3136***	0.3179***
	(0.0556)	(0.0564)
Protected x Hurricane	0.0765*	0.0591
Trotected x Trufficanc	(0.0312)	(0.0303)
Fixed-Effects:		
Year	Yes	Yes
Property	Yes	Yes
S.E.: Clustered	Property	Property
Observations:	3,172	3,172
	*	

Note: standard errors in parentheses; ***p < 0.01, **p < 0.05, *p < 0.1

Table 2.8 reports the full results of the pooled regression with neighbourhood (census block group) fixed effects as referenced in the main text. The model includes a comprehensive set of property characteristics, environmental variables, and interaction terms, allowing for a comparison with the property fixed effects specification.

Table 2.8: Neighbourhood Fixed Effects Regression Output

	Model 7	Model 8
	(All within 1K)	(All within 1K)
Variables	log(price)	log(price)
	0.0345	0.0332
Protected (=1)	(0.0259)	(0.0260)
	0.0568***	0.0634
Hurricane (=1)	(0.0210)	(0.0352)
	-0.0571***	-0.0571***
Protected X Hurricane	(0.0153)	(0.0154)
	-0.0117***	-0.0117***
Age	(0.0011)	(0.0011)
	8.16e-5 ***	8.15e-5***
Age square	(1.42e-5)	(1.41e-5)
	0.0001***	0.0001***
Total Area	(5.72e-6)	(5.67e-6)

Bedrooms	0.0200* (0.0078)	0.0191* (0.0077)
D 4	0.0848***	0.0850***
Bathrooms	(0.0091)	(0.0091)
	0.0648**	0.0654**
Garage (=1)	(0.0216)	(0.0215)
. , ,	-0.0495**	-0.0460*
Carport (=1)	(0.0186)	(0.0186)
D 1(1)	0.0636***	0.0614***
Pool (=1)	(0.0124)	(0.0123)
D (1.1 (1)	0.0250*	0.0228
Boat dock (=1)	(0.0124)	(0.0123)
G 11 (1)	0.2893***	0.2924***
Seawall (=1)	(0.0273)	(0.0271)
	-0.0640***	-0.0661***
Stories	(0.0176)	(0.0175)
E14:	0.0535***	0.0537***
Elevation	(0.0142)	(0.0141)
D:-4	-0.0214	-0.0226
Distance to school	(0.0299)	(0.0296)
Distance to bealth and	0.0369	0.0379
Distance to healthcare	(0.0448)	(0.0455)
Distance to Supermarket	-0.0280	-0.0288
-	(0.0415)	(0.0415)
Distance to Recreation	-0.0444*	-0.0452*
centre	(0.0219)	(0.0220)
Distance to Park	0.0228	0.0227
	(0.0276)	(0.0272)
	-0.1091***	-0.1096***
Distance to coastline	(0.0143)	(0.0143)
	0.0101	0.0118
Flood Zone (=1)	(0.0145)	(0.0145)
Fixed-Effects:		
Year	Yes	No
Quarter-year	No	Yes
Census Block level	Yes	Yes
S.E.: Clustered	Census block	Census block
Observations:	19,234	19,234
R2	0.75176	0.75388
N-4411		< 0.01 **** < 0.05

Note: standard errors in parentheses; ***p < 0.01, **p<0.05, *p<0.1

Chapter 3

Let 'Em Grow: Do Florida Coastal Property Owners Value Mangroves?

3.1 Introduction

Coastal zones comprise only 4% of the Earth's land area and 11% of ocean surface, yet they are among the planet's most ecologically and economically productive regions. These areas provide life-sustaining ecosystem services, including food provision, nutrient cycling, and storm buffering (Barbier et al., 2013; Millennium Ecosystem Assessment, 2005). Yet these ecosystems face growing pressure from human activity, particularly as population growth accelerates in coastal areas. Their low-lying geography and exposure to tropical storms, sea-level rise, and coastal erosion render them particularly vulnerable to natural hazards. In the United States, coastal counties account for 40 percent of the population, with a 40 percent increase recorded between 1970 and 2010 (National Oceanic and Atmospheric Administration, Office for Coastal Management, 2013). This rapid expansion in hazard-prone areas heightens the need to protect and preserve natural coastal buffers - such as mangroves, which offer cost-effective protection against storm surge and flooding. The increasing exposure of assets and communities to coastal risks makes the conservation of these natural defenses not only ecologically important but also economically and socially imperative.

Mangroves are a highly productive and salt-tolerant coastal forest ecosystem found primarily in the tropical and sub-tropical intertidal regions of the world. Globally, mangroves reduce property damage by an estimated \$65 billion annually and protect over 15 million people from coastal flooding (Menéndez et al., 2020). This study investigates whether and how the presence of mangroves is capitalized into coastal property values along Florida's Gulf Coast. We adopt a

property fixed effects hedonic pricing model and employ a long-difference framework, linking repeat sales housing data with geospatially referenced mangrove extent from the Global Mangrove Watch (GMW) (Bunting et al., 2018, 2022) for three time points: 1996, 2007, and 2017. This approach enables us to examine how the effect of mangrove proximity on property values evolves over time, providing insight into the dynamic relationship between environmental amenities and housing markets. The analysis focuses primarily on the proximity to mangroves, measured as the logarithm of distance to the nearest mangrove patch. This variable captures the most direct spatial relationship between each property and adjacent mangrove coverage and serves as the core measure of mangrove exposure across counties and time. In a supplemental analysis for one of the study counties, we also incorporate two additional spatial dimensions, mangrove area within a buffer radius of the property and viewshed-based mangrove visibility, to explore whether these features are differentially capitalized into housing values.

A substantial body of research has examined the protective services provided by coastal ecosystems, particularly in reducing storm-related damages and preserving lives. Barbier & Enchelmeyer (2014) used the expected damage function framework to estimate the economic value of storm protection provided by wetlands, showing that even a 0.1 unit increase in wetland continuity per meter can reduce storm-related damages by \$99–\$133 per sub-planning unit. Sun & Carson (2020) used the expected damage function approach to assess the economic value of wetlands in mitigating damage resulting from 88 tropical storms and hurricanes that hit the United States between 1996 and 2016. Del Valle et al. (2020) and Hochard et al. (2019, 2021) used remote sensing data to show that areas with mangrove buffers in the US and globally experienced smaller economic disruptions and faster recovery following coastal storms. Studies related to India's 1999 super cyclone (Das & Crépin, 2013; Das & Vincent, 2009) found that continuous mangrove belts

were associated with significantly fewer fatalities and substantially reduce structural damage even at considerable distances from both the mangroves and the coastline. Together, these studies highlight the role of mangroves as critical ecological infrastructure in mitigating storm impacts. However, most of this work focuses on outcomes at regional or community scales, leaving open the question of whether and to what extent such protective benefits are reflected in individual housing market outcomes.

Hedonic pricing provides a well-established framework for estimating the implicit value of nonmarket environmental goods, including those related to coastal protection and aesthetic quality. Prior studies have used hedonic methods to value beach quality (Landry & Hindsley, 2021), beach nourishment (Gopalakrishnan et al., 2011), dune restoration (Dundas, 2017) and voluntary property buyouts (Hashida & Dundas, 2023). It has also been used to assess the impact of flood risk and coastal amenities on housing markets (Atreya et al., 2013; Atreya & Ferreira, 2015; Bakkensen et al., 2019; Bakkensen & Barrage, 2022; Bin, Kruse, et al., 2008; Kousky, 2019). A growing body of research also highlights the importance of incorporating viewshed analysis in hedonic pricing models, particularly in environmental valuation (Bin et al., 2008; Dundas, 2017; Hamilton & Morgan, 2010; Paterson & Boyle, 2002; Walls et al., 2015). When visibility of an environmental amenity is correlated with other spatial features, omitting it can lead to biased estimates of amenity values. Several studies have used high-resolution elevation data, such as Light Detection and Ranging (LiDAR), to construct viewshed-based variables. In coastal contexts, ocean views have been shown to significantly influence property values. Bin et al. (2008) and Hamilton & Morgan (2010) estimate households' willingness to pay for incremental improvements in ocean views, while Dundas (2017) finds effects of ocean visibility in the context of dune restoration. Other studies assess the impact of views of terrestrial land cover. Paterson & Boyle (2002) and Walls et al. (2015) found mixed results, with forest views negatively affecting prices in some cases, while farmland views having positive effects. Sander & Polasky (2009) emphasize that both the composition and diversity of visible land cover types also matter for valuation. Consistent with earlier work that relies on visibility metrics, we incorporate a viewshed-derived index of mangrove visibility to assess whether and to what extent, visible mangroves are capitalized into housing prices.

Biophysical studies have demonstrated the protective capacity of mangroves, however empirical evidence on whether such benefits are reflected in housing markets is limited. This paper addresses this gap by applying a property-level hedonic pricing model to evaluate whether housing prices respond to changes in mangrove exposure. Our analysis reveals that over the initial ten years, a 1% increase in distance from mangroves is associated with a 0.007% to 0.06% increase in property prices across the two counties. However, this relationship does not persist over a longer time horizon, suggesting that the influence of mangrove proximity on housing prices diminishes over time. We find no consistent evidence that mangrove areal extent or visibility affects property prices.

Our study contributes to the growing literature on the economic valuation of ecosystem services provided by mangroves and wetlands. Prior work has primarily focused on estimating the protective value of mangroves in the context of natural hazards, including studies in India (Das & Crépin, 2013; Das & Vincent, 2009), Thailand (Barbier, 2008) and the USA (Del Valle et al., 2020; Narayan et al., 2019; Sun & Carson, 2020). While these studies highlight the storm protection benefits of mangroves, they do not directly assess how such ecosystems are valued in housing markets. To the best of our knowledge, ours is the first hedonic pricing study to incorporate fine-scale spatial proxies of mangrove presence specifically, proximity, area within a defined radius,

and visibility from individual properties, to estimate their capitalization into coastal property values.

3.2 Study Area

Florida boasts an estimated 600,000 acres of mangrove forests, representing the largest extent of these ecosystems in the continental United States (Florida Department of Environmental Protection, 2024). The three species found in Florida — red mangrove (Rhizophora mangle), black mangrove (Avicennia germinans), and white mangrove (Laguncularia racemosa), each have unique characteristics and occupy different parts of the coastal environment. Red mangroves, with their distinctive prop roots, typically grow along the water's edge, while black mangroves occupy slightly higher elevations and can be identified by their finger-like projections called pneumatophores. White mangroves usually grow upland from the other two species. Our study focuses on the southwest coast of Florida, particularly the Tampa Bay region, that has experienced significant urbanization in the last few decades. This region, which encompasses Florida's largest open-water estuary, has witnessed a substantial loss of coastal wetlands. According to the Southwest Florida Water Management District (Garcia et al., 2023) there has been a loss of over 44% of the wetlands bordering Tampa Bay in the past century. Analyzing the effects of changes in mangrove extent over time in this region is crucial, given its environmental significance and the scale of the observed habitat loss.

This study focuses on Pinellas and Hillsborough counties (Figure 3.1), located along Florida's Gulf Coast and bordering the Tampa Bay estuary. According to the 2020 U.S. Census, Pinellas is the fourth most populous county in the state, with 959,107 residents and a population density of 3,512.8 people per square mile. It has 442,789 occupied housing units and a homeownership rate

of 68.3%, slightly above the state average. Hillsborough County is larger and more populous, with 1,513,301 residents and a population density of 1,480 people per square mile. It contains 559,949 occupied housing units but has a lower homeownership rate of 61.2%. Median household income in Hillsborough is \$74,308, above the state median, while in Pinellas it is slightly lower at \$66,472. Both counties are ecologically and economically significant, but they differ in landscape characteristics and coastal exposure. Pinellas County is highly urbanized and defined by its extensive Gulf coastline and low-lying coastal zones. Hillsborough County, by contrast, features a more diverse natural landscape, including inland river systems, forests, and wetlands. Although its mangrove coverage is more spatially dispersed, these ecosystems still play a vital role in the county's coastal resilience. The contrasting ecological and development patterns across the two counties provide a valuable setting for examining how proximity to mangroves is capitalized in their residential housing markets.

3.3 Empirical Strategy

We estimate the relationship between housing prices and mangrove proximity using a long-difference specification based on a repeat sales transaction. This approach compares changes in housing prices over extended intervals, specifically between 1996, 2007, and 2017, to assess whether shifts in proximity to mangroves are capitalized into property values. Following Chay & Michael (2005), study of the Clean Air Act's county-level reductions in total suspended particulates, which treats the 1970 and 1980 census observations as two post-adjustment equilibria, we assume the ten-year change in housing prices as households' long-run willingness to pay for the environmental amenity. By focusing on long time horizon, the model captures changes in housing market outcomes while differencing out time-invariant unobserved heterogeneity.

Our core specification follows a semi-log form, standard in the hedonic valuation literature, to account for the skewed distribution of housing prices and to allow coefficient interpretations in percentage terms (Kuminoff et al., 2010). The primary variable of interest is the logarithm of the distance to the nearest mangrove patch, capturing spatial proximity to mangrove extent. The property fixed-effects specification is presented in Equation (1):

$$ln(P_{it}) = \beta_0 + \beta_m \left(log(distance \ to \ mangroves_{it}) * Period_t \right) + \alpha_i + \varepsilon_{it} \tag{1}$$

where P_{it} is the inflation-adjusted sale price of the property i in year t. The primary variable of interest is the interaction term $log(distance\ to\ mangroves_{it})*Period_t$, where $log(distance\ to\ mangroves)$ represents the log of the distance from the property to the nearest mangroves and Period_t is an indicator for the 2007 and 2017 periods, with 1996 as the reference year. The terms α_i captures unobserved, time-invariant property-specific effects (Livy & Klaiber, 2016; Palmquist, 1982) and ε_{it} is the idiosyncratic error term. We also estimate a pooled regression model, incorporating a range of property characteristics alongside the $distance\ to\ mangroves$ variable. To account for localized unobserved heterogeneity, we include census block-level fixed effects.

While long difference models effectively eliminate time-invariant characteristics, they do not account for time-varying neighborhood factors that may influence housing prices and correlate with mangrove proximity. As part of the future work, we plan to extend the analysis by incorporating neighborhood-level controls, as outlined in Equation (2).

$$\Delta ln(P_{ic}) = \beta \Delta (log(distance\ to\ mangroves_{ic})) + \gamma' \Delta N_{ic} + \eta_c + \varepsilon_{ic}$$
 (2) where $\Delta ln(P_{ic})$ is the change in the sale price of the property i in county c between the years 1996 and 2007. $\Delta (log(distance\ to\ mangroves_{ic}))$ is the change in the proximity to the nearest

mangroves patch; ΔN_{ic} is a vector of changes in neighbourhood-level covariates and η_c controls for unobserved county level trends. This approach is conceptually similar to that of <u>Taylor & Druckenmiller (2022)</u> who used a long-difference model to evaluate NFIP claims at the ZIP code level, incorporating state fixed effects and a rich set of control variables capturing socio-economic changes. While the authors don't explicitly state market equilibrium, their long-difference methodology implicitly assumes it.

To further explore whether alternative measures of mangrove exposure influence housing prices, we estimate additional models using a subset of the data restricted to repeat sales transactions between Period 0 (1994–1998) and Period 1 (2005–2007) in Pinellas County. All spatial exposure measures are constructed within a 1km buffer radius of each property. The choice of a 1 km extent is guided by existing literature, <u>Bin et al.</u> (2008) use a 1-mile viewshed buffer in their study of coastal amenities.

Area Analysis

Using ArcGIS Pro, we generate 1 km buffer around each property and intersect them with mangrove extent layers to estimate the total area of mangroves within each buffer radius. The *percent mangroves area* in equation (3) refers to the percentage of the mangrove within 1 km buffer around each property.

$$\ln(P_{it}) = \beta_0 + \beta_{\rm m} \left(\log(percent\ mangroves\ area) * {\sf Period}_{\sf t}\right) + \alpha_i + \varepsilon_{it} \tag{3}$$
 All other variables in Equation (3) are defined in earlier specifications.

Viewshed Analysis

To account for the visibility of mangroves from each property, we incorporate a viewshedbased measure of visual exposure into the hedonic model. Similar to the area-based analysis, this viewshed analysis is limited to Pinellas County and includes only repeat sales observed in just two periods: period 0 (1994-1998) and period 1 (2005-2007). The analysis is conducted in ArcGIS Pro using the VIEWSHED function, with inputs including property coordinates (as observer points), mangrove extent layers, and a custom digital elevation model (DEM) that accounts for both natural topography and built structures. Because standard DEMs do not reflect visual obstructions from buildings, we construct year-specific terrain surfaces that incorporate vertical structures. Building height data are derived from GIS parcel shapefiles, with the number of stories assigned to each structure. Following Sander & Polasky (2009), we assume an average floor height of 3 meters and add 2 meters to account for roof and foundation elevations. The resulting raster layer is added with a base 10-meter DEM (USGS Earth Explorer) to create an elevation surface that reflects both topography and built structures. To reflect changes in the built environment, we construct separate DEMs for 1996 and 2007, using building data available for each period. We calculate the viewshed from each property within a 1-kilometer radius using the year-specific custom DEM and mangrove extent for each period. In our viewshed analysis, the observer point is placed at the top of each building, approximating the highest occupied floor. No additional observer height is added. Figure 3.2 illustrates the viewshed analysis for a representative property. A 1-kilometer buffer (shown in blue) is drawn around the parcel to define the spatial extent of the viewshed. Using the customized elevation surface, the viewshed function is applied to identify all areas visible from the top-story window of the house. The resulting visible region is highlighted in orange. Mangrove extent, shown in light green, is then overlaid with the viewshed output. The intersecting area, representing the portion of mangroves visible from the property, is shown in yellow and used to calculate the percentage of mangrove area that is visible within the 1-kilometer radius.

$$ln(P_{it}) = \beta_0 + \beta_m (log(percent \ viewshed \ area) * Period_t) + \alpha_i + \varepsilon_{it}$$
 (4)

All variables in Equation (4) are as defined in earlier specifications. The term *percent viewshed area* refers to the percentage of the visible mangrove area within a 1 km buffer around each property. We also estimate two additional specifications: one that includes both percent mangrove area and proximity, and another that pairs viewshed with proximity.

In practice, the scope of our analysis is shaped by data availability. The Global Mangrove Watch dataset provides consistent spatial coverage for mangrove extent beginning in 1996, with additional layers available for 2007 and subsequent years. Consistent with prior studies (<u>Walls et al., 2015</u>), which link land cover data from a single year to nearby years of sales transactions, we use static mangrove extent layers for representative periods. Specifically, as indicated in Table 3.1, we link the 1996 GMW mangrove layer to housing transactions from 1994 to 1998, and the 2007 layer to transactions from 2005 to 2007, and the 2017 layer to transactions from 2015 to 2018. Based on this approach, our main analysis focuses on three discrete periods to evaluate long-term changes in the relationship between mangrove proximity and housing prices.

3.4 Data & Descriptive Statistics

The primary data source for this study is the property sales records obtained from the Pinellas and Hillsborough County's Property Appraiser's website. We focus on single-family home sales that align with the years of the available Global Mangrove Watch (GMW) dataset. To construct the first long-difference period (1996 to 2007), we use sales from 1994–1996 to represent the baseline period and sales from 2005–2007 to represent the later period. For the second long-difference period (1996 to 2017), we pair the same baseline window (1994–1996) with sales from 2015–2017. This structure allows us to estimate price changes over roughly 10-year and 20-year intervals, anchored to the timing of available mangrove extent data.

To adjust for inflation, housing prices are deflated using the Housing Price Index for respective Counties, sourced from the Federal Reserve Economic Data (FRED), and expressed in 2019 dollars. Shapefiles containing property identification numbers and geographic coordinates were downloaded from the respective County's Open data portal. Lastly, elevation data from the USGS Earth Explorer is used to construct terrain surfaces, which are critical for conducting viewshed analysis.

Table 3.2 summarizes the descriptive statistics for key variables used in the long-difference analysis, separately for Pinellas and Hillsborough. The sample includes all repeat sales of single-family homes located within 2 km of either mangrove or the ocean as shown in Figure 3.3. Mean sales prices were higher in Hillsborough County, averaging \$462,000 compared to approximately \$358,000 in Pinellas County. While several structural features—such as docks, fireplaces, pools, and porches—are recorded only for Pinellas, Hillsborough includes other characteristics such as the number of bedrooms and bathrooms, heated area, and lot size, reflecting differences in available data across the two property appraiser systems. In terms of structural features, homes in both counties are predominantly single-unit and single-story dwellings, though Hillsborough properties tend to be newer on average (mean age of 32.5 years in Hillsborough vs. 40.5 years in Pinellas). With respect to environmental characteristics, properties in Hillsborough are generally farther from mangroves, mean distance of 12,570 feet vs. 10,251 feet in Pinellas. Elevation levels are comparable across the two counties.

For the subsample analysis using alternative mangrove exposure measures, the subset includes 1,752 repeat-sale observations located within 1 km buffer. We note that the exposure to mangroves—whether measured by area or visibility—is sparse for a majority of properties. The average mangrove area within 1 km of property is approximately 185,429 square feet, but the

median and first quartile are both zero, and over 75% of properties have less than 29,000 square feet of mangroves nearby. In percentage terms, the average coverage within the 1 km buffer is 0.55%, with a maximum of 15.7%, reflecting a highly skewed distribution. The viewshed-based metrics show comparable patterns. The average visible mangrove area within 1 km is roughly 185,653 square feet, while both the median and first quartile remain zero. The mean percentage of visible mangrove area is 0.55%, nearly identical to the buffer-based measure, with a maximum of 15.7%. These distributions highlight the substantial heterogeneity in mangrove exposure across properties, with a concentration of observations clustered at or near zero exposure.

3.5 Results

The analysis uses a long-difference framework across three periods (1996, 2007, and 2017) and draws on data from two coastal counties: Pinellas and Hillsborough. We focus exclusively on repeat sales of properties located within 2 km of either mangroves or the ocean, restricting the sample to those sold multiple times during the study window. This approach enables the estimation of within-property changes in housing prices while controlling for all time-invariant, unobserved characteristics. Table 3.3 presents the results from property fixed-effects regressions, with standard errors clustered at the census block level.

In Pinellas County, the interaction between distance to mangroves and the first long-difference period (a 10-year change from 1996 to 2007) is positive and statistically significant. This suggests that over the first long difference period, homes located farther from mangroves are appreciated more than those nearby, indicating a price penalty associated with proximity to mangroves. However, in the extended long-difference period (the 20-year change from 1996 to 2017), the interaction term is statistically insignificant, implying that this effect has faded over time. A similar

pattern is observed in Hillsborough County. The first long-difference period (1996–2007) shows a strong positive association between distance to mangroves and housing prices but by the 20-year mark (1996–2017), the effect reverses and becomes marginally significant, suggesting a potential shift in market preferences toward valuing proximity to mangroves. Future research will explore the drivers of this shift by integrating neighborhood-level characteristics into the long-difference framework, as specified in Equation (2).

Taken together, the results point to a temporal shift in how mangrove proximity is valued in the housing market. To complement the main analysis, we estimate a pooled model that includes structural characteristics and neighborhood fixed effects. The estimated coefficients align with expectations – property prices decrease with age and with increasing distance from the coastline. The effect of mangrove proximity is similar in both magnitude and direction to that observed in the property fixed-effects model, particularly in the first 10-year long-difference specification. The results are presented in Table 3.4 in Appendix B.

We run the subsample analysis of properties in Pinellas County located within 1 km of either the coastline or the mangrove fringe. Repeat-sales models with property fixed effects are estimated with *percent mangroves area* and *percent viewshed area* as key explanatory variables. In both cases, the coefficients are small and statistically insignificant, suggesting no discernible relationship between these areal measures and housing prices. As a robustness check, we estimate pooled OLS models that include mangrove proximity along with each areal variable. Across all pooled specifications, proximity to mangroves remains statistically significant and consistent in magnitude, while the *percent mangroves area* and *percent viewshed area* measures continue to show no meaningful effect. These findings indicate that it is the proximity to the

mangrove patch and not the total area or visibility of mangroves within 1 km of a property, that is priced into the housing market. Detailed pooled results are reported in Table 3.5 of Appendix B.

3.6 Discussion

This study investigates the relationship between mangrove proximity and housing prices using a long-differences framework applied to repeat sales data. The results reveal a positive and statistically significant association between distance to mangroves and property values over the initial ten-year period (period 1 relative to period 0), suggesting that closer proximity may be perceived as disamenity. However, when the analysis is extended to a longer horizon, spanning 20 years, the effect of mangrove proximity becomes statistically insignificant. This temporal divergence indicates that the initial disamenity effect associated with mangrove proximity diminishes over time. Several factors may contribute to this attenuation. One possible explanation is the impact of policy interventions, notably Florida's Mangrove Trimming and Preservation Act (MTPA, 1996). This legislation, which restricts mangrove trimming and imposes penalties for non-compliance, was enacted to preserve the ecological benefits of mangroves, including their role in storm surge protection. While disentangling this effect is beyond the scope of this study, primarily due to limitations in historical mangrove data. The findings, however, highlight the dynamic nature of how environmental amenities and disamenities are capitalized in housing markets. The fading of the negative proximity effect may reflect shifting public perceptions, increased environmental awareness, or more effective regulatory enforcement in urban coastal areas.

Looking ahead, there is a clear need for high-resolution, annual mangrove extent datasets to support more granular analyses of these dynamics. Emerging advancements in remote sensing and machine learning classification provide promising tools for generating such time series. Future research that integrates these spatial datasets with detailed property transaction records can more precisely identify the long-term market effects of mangrove coverage and assess the influence of environmental policy. Despite current data constraints, this study lays groundwork for future research at the intersection of land markets, ecosystem change, and coastal management.

Table 3.1: Correspondence of Mangrove Extent Years to House Sale Years

GMW Year	Sales Year Range
1996	1994 – 1998
2007	2005 - 2007
2017	2015 - 2019

Note: GMW refers to the Global Mangrove Watch dataset. Mangrove extent layers from each reference year are linked to nearby housing transactions to represent property proximity to mangroves.

Table 3.2: Descriptive Statistics

Variables	Pinellas		Hillsborough	
	Mean	SD	Mean	SD
Sales Price (\$1000)	357.83	284.68	461.67	620.41
dock (1/0)	0.085	0.279	-	-
Fireplace (1/0)	0.496	0.500	-	-
Pool (1/0)	0.515	0.500	-	-
Porch (1/0)	0.049	0.215	-	-
Total Effective Area (sq ft)	2251.76	1252.49	-	-
Units	1.01	0.12	1.03	0.16
Stories	1.27	0.52	1.31	0.54
Age	40.51	20.05	32.50	28.00
Beds	-	-	3.30	0.86
Baths	-	-	2.33	0.95
Heated area	-	-	1973.34	1017.55
Acreage	-	-	0.23	0.33
Distance to mangroves (ft)	10251.10	6901.77	12569.88	8554.58
Distance to coastline (ft)	2626.07	1966.55	1534.83	1019.46
Elevation (m)	11.25	6.07	11.17	5.52

Table 3.3: Property Fixed Effects Regression

	Pinellas	Hillisbourg
	Model 1	Model 2
Variables	log (price)	log (price)
log (Distance to	0.0071*	0.0595***
mangroves) $x period = 1$	(0.0030)	(0.0077)
log (Distance to	-0.0046	-0.0238*
mangroves) $x period = 2$	(0.0061)	(0.0116)
Fixed-Effects:	, , ,	· · · · · · · · · · · · · · · · · · ·
Property	Yes	Yes
S.E.: Clustered	Census Block	Census Block
Observations:	7,997	26,553
R2	0.87386	0.83827

Note: standard errors in parentheses; ***p < 0.01, **p < 0.05, *p < 0.1

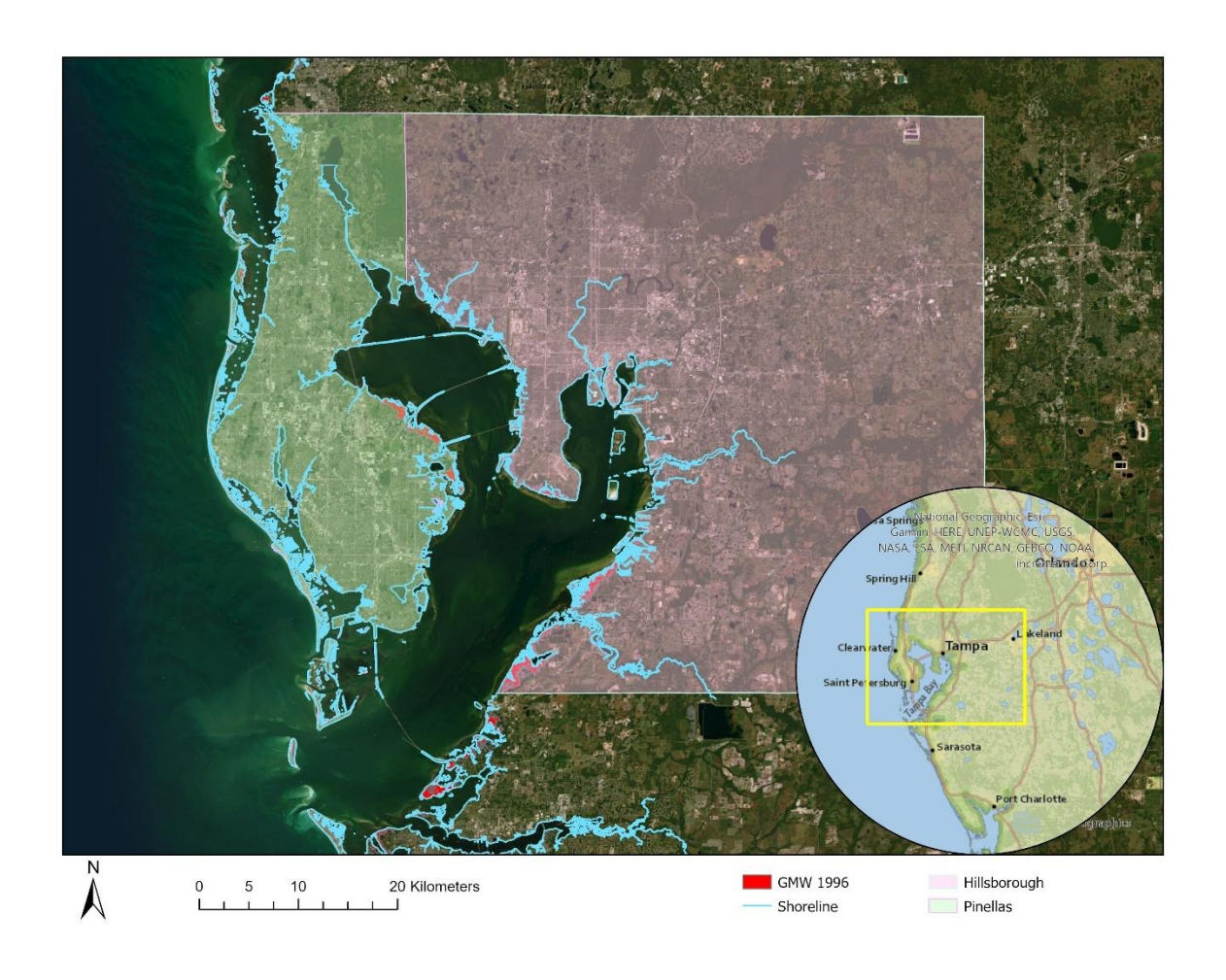


Figure 3.1: Study Area - Pinellas and Hillsborough County, Florida

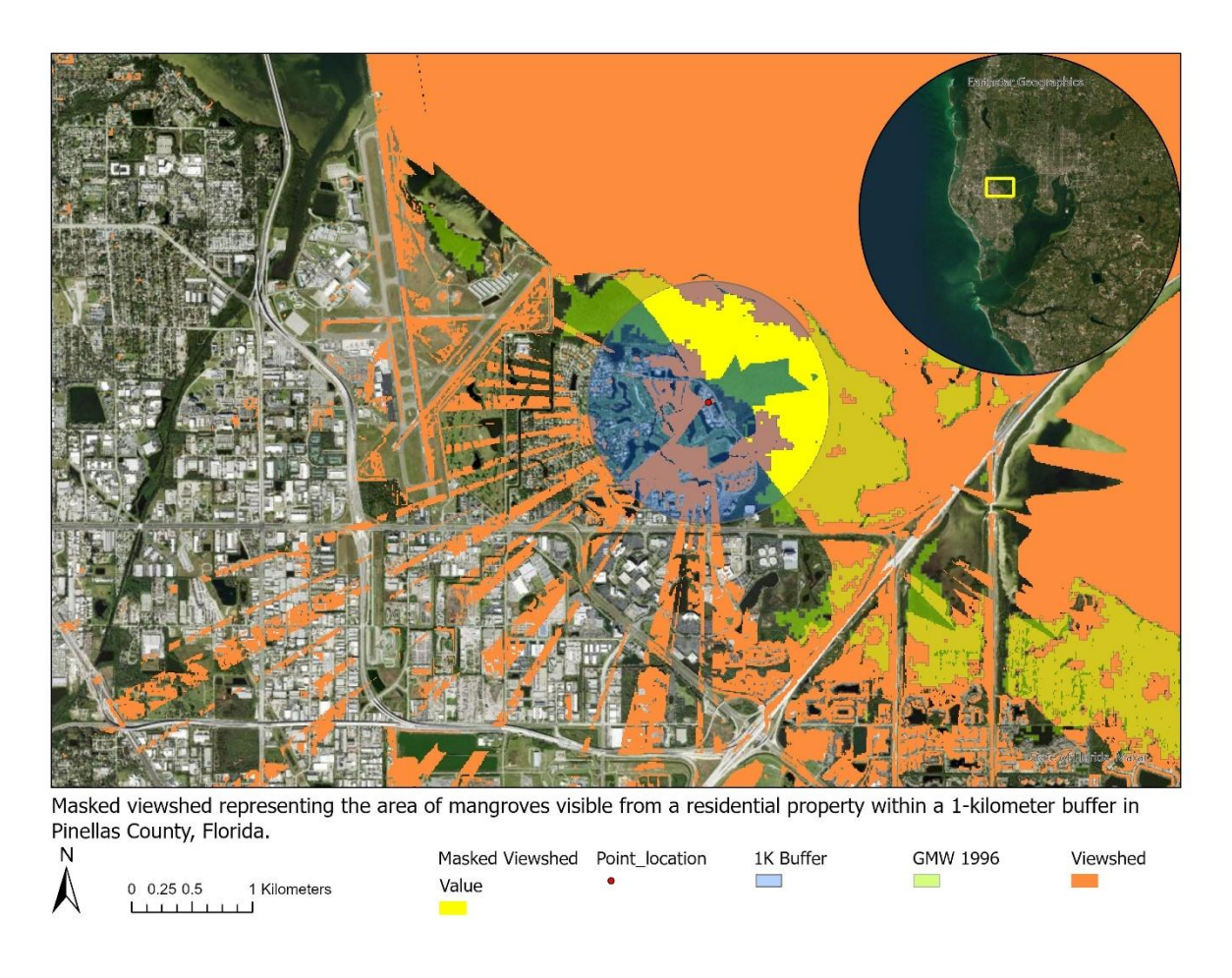


Figure 3.2: Visibility analysis for a representative property, showing buffer, viewshed, mangroves, and visible mangrove extent.

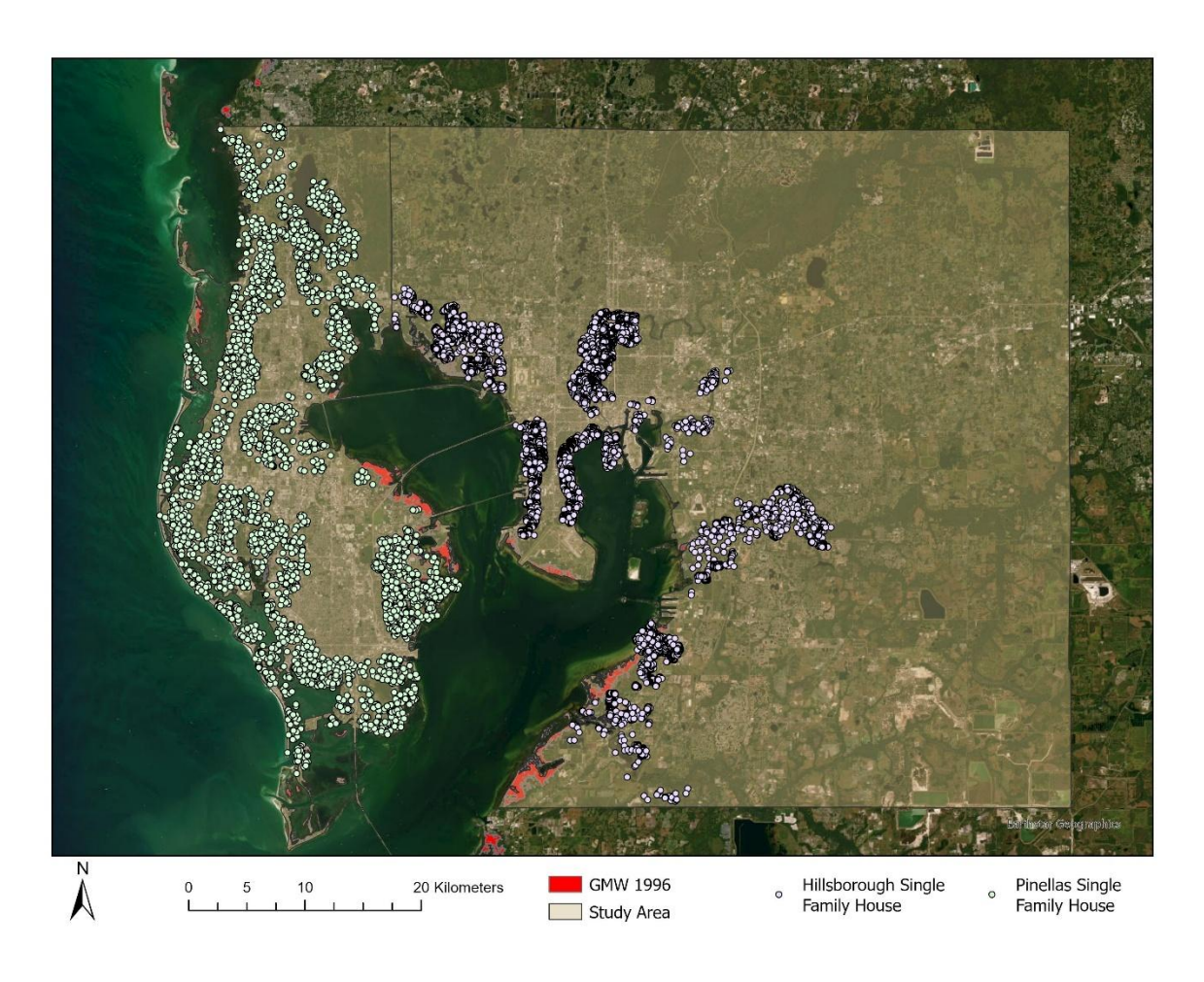


Figure 3.3: Repeat sales within 2K buffer

Appendix B

Table 3.4: Pooled Regression Output using Proximity measure only

_	Pinellas		Hillisbourg	
	Model 1	Model 2	Model 3	Model 4
	(1K Buffer)	(2K buffer)	(1K Buffer)	(2K buffer)
Variables	log (price)	log (price)	log (price)	log (price)
log (Distance to	0.0234***	0.0174***	0.1242***	0.1193***
mangroves) $x period = 1$	(0.0021)	(0.0019)	(0.0016)	(0.0021)
log (Distance to	0.0225***	0.0173***	0.1158***	0.1070***
mangroves) $x period = 2$	(0.0038)	(0.0034)	(0.0018)	(0.0018)
A 00	-0.0042**	-0.0033*	0.0019***	0.0019***
Age	(0.0016)	(0.0015)	(0.0005)	(0.0004)
$\operatorname{Dod}_{r}(0/1)$	0.2133***	0.2101***		
Dock (0/1)	(0.0387)	(0.0392)		
Fina (0/1)	0.1152***	0.1094***		
Fire (0/1)	(0.0215)	(0.0185)		
P 1 (1/0)	0.1678***	0.1669***		
Pool (1/0)	(0.0208)	(0.0174)		
D 1 (1/0)	0.0836.	0.0838*		
Porch (1/0)	(0.0429)	(0.0333)		
11 '4 (1/0)	-0.0222	-0.1443	-0.1235*	-0.1042**
Units (1/0)	(0.2304)	(0.1854)	(0.0493)	(0.0371)
S . :	-0.0423	0.0006	0.0240	0.0113
Stories	(0.0286)	(0.0327)	(0.0242)	(0.0189)
T / 1 F CC /	0.0001***	0.0001**	, ,	,
Total Effective Area	(2.64e-5)	(3.6e-5)		
1 (D: 4)	-0.0518*	-0.0635**	-0.1958***	-0.1823***
log (Distance to ocean)	(0.0247)	(0.0223)	(0.0289)	(0.0246)
Elevation	-0.0108	-0.0192	-0.0488**	-0.0513***
	(0.0214)	(0.0190)	(0.0169)	(0.0136)
log (Distance to ocean) x	0.0015	0.0029	0.0068**	0.0068***
elevation	(0.0031)	(0.0025)	(0.0025)	(0.0018)
D - 1-	, , ,	,	0.0476***	0.0415***
Beds			(0.0115)	(0.0093)
Baths			0.0364*	0.0334**

Heated Area			(0.0142) 0.0001*** (3.39e-5)	(0.0110) 0.0002*** (2.91e-5)
Acreage			0.0743* (0.0308)	0.0816** (0.0273)
Fixed-Effects:				
Census Block	Yes	Yes	Yes	Yes
S.E.: Clustered	Census Block	Census Block	Census Block	Census Block
Observations:	5,030	7,997	15,718	26,553
R2	0.85937	0.84215	0.75509	0.73136

Note: standard errors in parentheses; ***p < 0.01, **p<0.05, *p<0.1

Table 3.5: Pooled Regression Output for Pinellas Conty using area and viewshed measure

	Area analysis	Viewshed analysis	Area with proximity	Viewshed with proximity
Variables	log (price)	log (price)	log (price)	log (price)
log (Distance to			0.0227***	0.0227***
mangroves) $x period = 1$			(0.0043)	(0.0043)
(Percent of viewshed		-0.0025		-0.0006
area) $x period = 1$		(0.0047)		(0.0045)
(Percent of mangroves	-0.0025		-0.0007	
area) $x period = 1$	(0.0046)		(0.0045)	
A go	0.0144***	0.0144***	-0.0031	-0.0031
Age	(0.0017)	(0.0017)	(0.0038)	(0.0038)
Dock (0/1)	0.2484**	0.2484**	0.2516**	0.2516**
DOCK (0/1)	(0.0828)	(0.0828)	(0.0788)	(0.0788)
Fire (0/1)	0.0704	0.0704	0.0743	0.0743
THE (0/1)	(0.0534)	(0.0534)	(0.0467)	(0.0467)
Pool (1/0)	0.1668***	0.1668***	0.1260**	0.1260**
1 001 (1/0)	(0.0484)	(0.0484)	(0.0454)	(0.0454)
Porch (1/0)	0.2137	0.2136	0.1820	0.1820
1 oren (170)	(0.1261)	(0.1261)	(0.1193)	(0.1193)
Units (1/0)	-1.034***	-1.034***	-0.3964	-0.3962
Omts (1/0)	(0.1648)	(0.1648)	(0.2188)	(0.2188)
Stories	-0.1675*	-0.1674*	-0.1448*	-0.1448*
Stories	(0.0815)	(0.0814)	(0.0684)	(0.0684)
Total Effective Area	0.0003***	0.0003***	0.0003***	0.0003***
Total Effective Alea	(5.58e-5)	(5.58e-5)	(5.18e-5)	(5.18e-5)
log (Distance to ocean)	0.0103	0.0103	-0.0098	-0.0098

	(0.0574)	(0.0574)	(0.0597)	(0.0597)
Elevation	0.0355	0.0355	0.0370	0.0370
Elevation	(0.0469)	(0.0468)	(0.0360)	(0.0360)
log (Distance to ocean) x	-0.0041	-0.0041	-0.0044	-0.0044
elevation	(0.0067)	(0.0067)	(0.0054)	(0.0054)
Fixed-Effects:				
Census Block	Yes	Yes	Yes	Yes
S.E.: Clustered	Census Block	Census Block	Census Block	Census Block
Observations:	1,752	1,752	1,752	1,752
R2	0.85789	0.85789	0.862	0.862

Note: standard errors in parentheses; ***p < 0.01, **p < 0.05, *p < 0.1

Chapter 4

Shoreline Wonders: Navigating Mangroves with Geographic Information Systems

4.1 Introduction

Coastal ecosystems, although occupying just 4% of the Earth's land and 11% of its ocean surface, provide disproportionately large ecological and economic benefits. These include carbon storage, flood mitigation, water purification, and critical habitat for biodiversity. Yet, these regions—particularly coastal forests—are increasingly threatened by human activities. The U.S. coastal zone, which accounts for less than 10% of the country's land area, is home to nearly 40% of the population, making it especially vulnerable to land use pressures (National Oceanic and Atmospheric Administration, Office for Coastal Management, 2013). Between 1970 and 2010, the population in coastal counties grew by over 40%, driving intensified development and placing stress on natural buffers. As climate change amplifies risks such as storm surge and hurricane-induced flooding, the degradation of coastal forests raises critical concerns about the long-term resilience of coastal communities.

Occupying the intertidal zones of tropical and subtropical coasts, mangroves are salt-tolerant forests that play a critical role in protecting coastal areas. With their complex root systems, they stabilize shorelines, reduce erosion, trap sediments, and serve as critical barriers against storm surge and flooding. In addition to their protective role, mangroves support fisheries, store large amounts of carbon, and provide habitat for diverse flora and fauna. Despite these benefits, mangroves have experienced widespread loss due to coastal development, aquaculture, and climate-related stressors. Understanding how mangrove cover has changed over time is essential

for assessing both ecological resilience and the services these ecosystems provide to coastal communities. This study develops a remote sensing-based methodology to map the historical extent of mangroves in southwest Florida over the period 1985 to 2020 using the Google Earth Engine (GEE) platform. We use the Global Mangrove Watch (GMW) (Bunting et al., 2018, 2022) dataset as a reference and apply supervised learning approaches to predict mangrove extent.

Our approach builds on a growing body of research that leverages long-term satellite imagery to monitor mangrove extent and dynamics. The use of Landsat data has been central to this effort. Giri et al. (2011) pioneered the first high-resolution global mangrove map for the year 2000, using Landsat imagery to estimate a global extent of approximately 137,760 km² and highlighting regional hotspots of loss. This work laid the foundation for subsequent efforts such as the GMW (Bunting et al., 2018, 2022), which to produce consistent time-series maps of mangrove extent for select years starting 1996. With reported classification accuracy above 95%, the GMW dataset has become a widely used reference for both scientific research and conservation planning. The introduction of GEE has further expanded the capacity for large-scale, reproducible analysis of mangrove dynamics. Yancho et al. (2020) developed the tool to map and monitor mangrove ecosystems in Myanmar using a random forest classifier, showcasing GEE's utility in regional-scale ecosystem monitoring. Similarly, Lagomasino et al. (2021) used GEE and multisensor datasets to track mangrove loss and recovery following extreme climatic events, demonstrating the value of high-frequency observations in capturing both short-term disturbances and long-term trends. Together, these studies represent a significant shift from static snapshots to more dynamic, process-oriented assessments of mangrove change. In parallel, recent advances in deep learning have opened new frontiers in ecological remote sensing. Guo et al. (2021) introduced ME-Net, a mangrove extraction model trained using semantic segmentation and visual

interpretation of high-resolution Sentinel imagery. <u>Yang et al. (2022)</u> demonstrated the effectiveness of convolutional neural networks (CNNs) for mapping urban tree crowns using Landsat 8 imagery. While these approaches remain relatively underutilized in mangrove research, they highlight the growing potential of deep learning techniques for improving pixel-level classification accuracy, an aspect particularly relevant for applications requiring fine spatial granularity, such as ecosystem valuation.

A comprehensive, long-term analysis of mangrove extent in southwest Florida, capturing multidecadal trends, regulatory shifts, and development pressures, has been largely missing from
literature. This study addresses that gap by building a consistent temporal record of mangrove
cover spanning from 1985 to 2020, using a reproducible, scalable classification workflow
grounded in remote sensing and cloud computing. In addition to generating spatial data for
ecological monitoring, these outputs are specifically designed to support downstream economic
analysis on the capitalization of mangrove protection in adjoining coastal property markets.
Recognizing the need for higher spatial precision, future work will focus on developing a U-Net
(Ronneberger et al., 2015) based deep learning model as a future extension. U-Net is a
convolutional neural network architecture designed for pixel-wise image segmentation,
particularly effective in capturing fine spatial details and preserving boundary information. The
following sections describe the study area, data sources, creation of training labels, model
development, post-classification processing and results from the three supervised models.

4.2 Study Area

Mangroves in the continental United States are predominantly found in Florida, which supports most of these forests. Florida is home to approximately 600,000 acres of mangrove forests,

representing the largest and most ecologically significant mangrove habitat in the U.S. (Florida Department of Environmental Protection, 2024). These forests are concentrated along the southern and southwestern coasts, where subtropical conditions support their year-round growth. The region is dominated by three native species - red mangrove (Rhizophora mangle), black mangrove (Avicennia germinans), and white mangrove (Laguncularia racemosa), each occupying distinct ecological zones along the coastal gradient. Red mangroves, known for their prominent prop roots, thrive along the shoreline and play a key role in stabilizing sediments. Slightly inland, black mangroves grow at higher elevations and are recognized by their vertical pneumatophores, which facilitate gas exchange in oxygen-poor soils. White mangroves typically occur even further inland, where tidal influence is reduced. Together, these species form a transitional buffer zone between terrestrial and marine environments, supporting a wide array of biodiversity and providing critical services such as erosion control, water filtration, and fish nursery habitat.

Our study focuses on the southwest coastal region of Florida, specifically the Tampa Bay area, which is bordered by Pinellas, Hillsborough, and Manatee counties (see Figure 4.1). These areas are ecologically significant, encompassing Florida's dynamic coastal wetlands, and are also among the most urbanized and rapidly developing regions in the state. The Tampa Bay estuary, Florida's largest open-water estuary, has been particularly impacted by land conversion, hydrological alterations, and infrastructure development. Historical assessments by the Southwest Florida Water Management District (Garcia et al., 2023) report a loss of over 44% of coastal wetland acreage in the region over the past century—a trend that includes both mangrove forests and salt marshes. Given this context, a detailed analysis of long-term mangrove cover change in southwest Florida is both timely and necessary. Identifying spatial patterns of gain and loss over the past

several decades not only contributes to understanding ecosystem responses to anthropogenic and climatic pressures but also informs local conservation and land-use strategies.

4.3 Data Sources

Recent advances in cloud computing have significantly improved researchers' ability to access, process, and analyze large volumes of geospatial data. Platforms such as GEE allow for scalable, real-time processing of satellite imagery and other spatial datasets without the need for local storage or high-performance computing infrastructure. Among the wide range of datasets available on GEE, Landsat and Sentinel are two of the most widely used Earth observation programs for monitoring land cover, vegetation dynamics, and environmental change. The Landsat program, jointly operated by the U.S. Geological Survey (USGS) and NASA, was launched in 1972 and provides a continuous record of Earth's surface. On the other hand, Sentinel satellites are more recent and designed to provide regular, systematic, and reliable data for environmental and natural resource monitoring. Sentinel-1 offers a spatial resolution of 5 to 20 meters, depending on the imaging mode, while Sentinel-2 provides a resolution of 10 to 60 meters, depending on the spectral band. However, for studies requiring long-term temporal coverage, such as ours, Landsat imagery is preferred due to its extensive historical archive. Landsat 5 (U.S. Geological Survey, 2020a) Thematic Mapper which operated from 1984 to 2013, provides data suitable for the earlier portion of our study period. For years from 1999 onward, we use imagery from Landsat 7 (U.S. Geological Survey, 2020b) Enhanced Thematic Mapper Plus, launched in 1999. Both collections offer surface reflectance products that are atmospherically corrected and well-suited for land cover classification. We use the Shuttle Radar Topography Mission (SRTM) digital elevation data (Farr et al., 2007) at a resolution of 1 arc-second (approximately 30m) to map and mask higher elevation

area (NASA Jet Propulsion Laboratory, 2013). To generate ground truth for model training, we use GMW products, which provide mangrove extent maps for discrete years: 1996, 2000, 2007, 2010, 2015, and 2020. Specifically, we use the GMW layers from 1996 and 2020 as reference data to create binary training labels: mangrove = 1, non-mangrove = 0 for supervised classification.

4.4 Methodology

Preprocessing Steps

This section outlines the geospatial and spectral preprocessing steps conducted prior to classification, as illustrated in the block diagram (Figure 4.2). The workflow begins with acquiring Landsat 5 and Landsat 7 surface reflectance imagery, which serve as the primary input for generating spectral features across the study period (1985–2020). Terrain information from the SRTM Digital Elevation Model is incorporated to restrict the analysis to low-lying coastal areas by masking out higher elevation zones that fall outside the mangrove-growing range. We use GMW layers from 1996 and 2020 as ground truth because they represent the temporal extremes of mangrove extent in the dataset. This allows the model to learn from the widest observed variation in mangrove coverage, enhancing its ability to generalize across different spatial and temporal conditions, while also avoiding the added complexity of incorporating multiple intermediate years. These layers are combined through logical operations, described in the following section, to produce binary labels (mangrove = 1, non-mangrove = 0). Spectral and elevation data are extracted for each labeled point, and the dataset is partitioned into training (70%), testing (15%), and external validation (15%) subsets. The trained machine learning model is then used to predict mangrove extent using satellite imagery for each year from 1985 to 2020, enabling consistent year-on-year classification.

Label Generation from known mangrove extents

We start with the geometry tool in GEE to define the spatial extent of our study area that encompasses the coastal boundaries of Pinellas, Hillsborough, and Manatee counties in the Tampa Bay region. To define ground truth, we use the GMW layers from 1996 and 2020, which represent the earliest and most recent GMW products currently available. The logical intersection of these two layers allows us to identify core mangrove areas that have persisted over a 24-year period. To reduce classification uncertainty along the edges, we apply a spatial filter that retains only interior pixels fully surrounded by mangrove cover as shown in Figure 4.3 (a).

To generate non-mangrove training labels, we first created a union of the GMW 1996 and 2020 layers, which captured all areas classified as mangroves in either year. This union captured both persistent and transitional zones and served as a conservative estimate of historical mangrove presence. To reduce the risk of mislabeling near boundaries, we applied a 50-meter buffer using a focal maximum filter to create a mangrove buffer around this union. We then defined our region of interest (ROI) by expanding the mangrove union to a 1000-meter buffer, capturing ecologically adjacent areas. The non-mangrove class was derived by subtracting the 50-meter mangrove buffer from the 1000-meter ROI, isolating pixels located between these two boundaries. This approach helped minimize boundary contamination while focusing on stable, ecologically distinct non-mangrove zones (Figure 4.3(b)). Figure 4.3(c) shows the final training labels, combining core mangrove areas (in green) and non-mangrove regions (in red) into a single binary classification layer, where landcover = 1 indicates mangrove and landcover = 0 indicates non-mangrove.

Deriving Spectral and Elevation Features for Classification

We used Landsat 5 imagery for the period 1985 to 1998 and Landsat 7 for 1999 to 2020. The year 2020 served as our baseline for model development, with the classification model trained on

imagery from this year and validated against the GMW 2020 extent layer to assess accuracy. The algorithm that performed best was then applied across all years to generate consistent historical mangrove extent maps. For the model building, we gathered Landsat imagery from January 1 to December 31, 2020. The imagery was cloud-masked, clipped to the study area, and aggregated into a single, cloud-free composite using a median reducer.

The spectral bands from these Landsat composites served as the covariates (independent variables) in the classification model. As part of feature engineering, we further derived a suite of spectral indices listed in Table 4.1, to enhance distinction between mangrove canopy, open water, and upland surfaces. Each index targets a distinct biophysical property relevant to mangrove ecology. The Normalized Difference Vegetation Index (NDVI) exploits the strong reflectance of healthy vegetation in the near-infrared and its absorption in the red portion of the spectrum (Tarpley et al., 1984). The Enhanced Vegetation Index (EVI) was developed to improve sensitivity in high biomass regions and reduce atmospheric and canopy background effects (A. Huete et al., 1999). The Soil Adjusted Vegetation Index (SAVI) further corrects for soil brightness in areas with sparse vegetation cover (A. R. Huete, 1988). The Green Chlorophyll Vegetation Index (GCVI) uses the green reflectance band to estimate chlorophyll concentration, particularly in the absence of a red-edge band (Gitelson et al., 2003). For water detection, the Normalized Difference Water Index (NDWI) uses green and near-infrared reflectance to estimate vegetation water content (Gao, 1996). The Modified NDWI (MNDWI) replaces the NIR band with SWIR to enhance open water detection, particularly in built-up region (Xu, 2006). The Land Surface Water Index (LSWI), which also uses NIR and SWIR bands, has been used in wetland studies to detect waterlogged vegetation and changes in leaf water content (Chandrasekar et al., 2010). Two mangrove-specific indices were also included: the Composite Mangrove Recognition Index (CMRI), defined as the

difference between NDVI and NDWI (Gupta et al., 2018), and the Modular Mangrove Recognition Index (MMRI), which combines absolute NDVI and MNDWI values to improve mangrove—non-mangrove separation (Diniz et al., 2019). To capture spectral characteristics of built-up or disturbed areas, the Enhanced Built-up and Bareness Index (EBBI) integrates SWIR, NIR, and thermal infrared bands to distinguish built-up surfaces from bare soil and vegetation (As-syakur et al., 2012). Additionally, simple spectral ratios were computed to support surface characterization: the Simple Ratio (SR), defined as NIR divided by red reflectance, is one of the earliest vegetation metrics (Jordan, 1969); the Ratio 5/4 (SWIR/NIR) and Ratio 3/5 (Red/SWIR) are commonly used to distinguish vegetative and non-vegetative surfaces based on relative spectral behaviour.

Together, these thirteen indices form a complementary feature set that, when stacked alongside the original Landsat spectral bands and elevation data, enhanced the model's ability to distinguish mangroves from other land cover types.

Refining the Area of Interest for Classification using Otsu Thresholding

To refine the region of interest (ROI) for classification, we adapted the method of <u>Donchyts et al. (2016)</u> which applies Canny edge detection (Canny, 1986) to identify boundary zones, and <u>Otsu (1979)</u> thresholding method to compute an optimal threshold for water detection using the Modified Normalized Difference Water Index (MNDWI) as shown in Figure 4.4. MNDWI enhances the spectral contrast between open water and non-water surfaces by combining green and shortwave infrared (SWIR) bands. Higher MNDWI values typically correspond to water bodies, while lower or negative values indicate land or built-up areas. Pixels in the ROI with MNDWI values below this threshold were classified as land, while those above it were identified as open water. The resulting mask defines the final classification area, as shown in Figure 4.4(b).

4.5 Experimental Setup

Training Dataset

To construct the training dataset, we overlaid the binary landcover labels from Figure 4.3(c) where landcover = 1 indicates mangrove and landcover = 0 indicates non-mangrove, onto the refined Region of Interest (ROI) defined in Figure 4.4(b). This overlay resulted in a complete dataset comprised of both the output labels and the input covariates, which included Landsat surface reflectance bands, derived spectral indices, and elevation data. On this composite image, we performed stratified random sampling, extracting 3,000 samples per class to ensure balanced representation of mangrove and non-mangrove pixels in the training set. To facilitate robust model evaluation, the sampled points were partitioned into training, testing, and validation subsets. Specifically, 70% of the points were allocated for training, 15% for testing, and the remaining 15% reserved for validation. Hyperparameter tuning for each model was conducted using the training and testing sets, allowing us to optimize performance while avoiding overfitting. The final validation set, held out entirely from the model-building process, serves as an out-of-sample check to assess the generalizability and robustness of each classifier across unseen regions.

Model Development

GEE has increasingly been used in land use and land cover (LULC) change studies, combining the platform's cloud computing capabilities with supervised machine learning (ML) algorithms such as Classification and Regression Trees (CART), Random Forests (RF), and Support Vector Machines (SVM) (Ganjirad & Bagheri, 2024; Gorelick et al., 2017; M et al., 2023). These models can be trained directly within the GEE JavaScript API environment using labelled input features and allow flexible hyperparameter tuning and model evaluation. In this study, we implemented

each of these algorithms on a common training dataset and optimized them through grid search over relevant hyperparameters to maximize classification performance.

The Classification and Regression Tree (CART) model (Breiman et al., 1984) is a decision tree-based algorithm that recursively partitions the data into homogeneous subsets based on feature values, resulting in a hierarchical tree structure for classification. We tuned two key hyperparameters: maxNodes, which controls the maximum number of terminal nodes and thus the model's complexity, and minLeafPopulation, which specifies the minimum number of samples required in a terminal node to reduce the risk of overfitting. A grid search was conducted over five values for each hyperparameter: maxNodes = {10, 50, 75, 100, 150} and minLeafPopulation = {5, 10, 20, 50, 100}, resulting in 25 total hyperparameter combinations. For each combination, the model was trained on the training set and evaluated on the testing set. Based on classification accuracy, the optimal hyperparameter values for the final CART model were maxNodes = 50 and minLeafPopulation = 20.

The next model we implemented was Random Forest (RF) (Breiman, 2001), an ensemble learning method that constructs multiple decision trees and aggregates their predictions to improve classification accuracy and reduce overfitting. We tuned three key hyperparameters: numberOfTrees, which determines the total number of trees in the ensemble; variablesPerSplit, which specifies the number of features randomly selected at each split to promote tree diversity; and bagFraction, which controls the proportion of training data sampled (with replacement) to grow each tree. A comprehensive grid search was conducted over 120 combinations, testing numberOfTrees values of 50, 100, and 150; variablesPerSplit values ranging from 5 to 14; and bagFraction values from 0.60, to 0.90. Each model was trained on the training set and evaluated on a validation set, with classification accuracy used as the selection criterion. The optimal

hyperparameter values for the final RF model were numberOfTrees = 50, variablesPerSplit = 12, and bagFraction = 0.60, which yielded an accuracy of 89.2%. The Variable Importance from the Random Forest model shown in Figure 4.5 highlight the importance of spectral indicators in distinguishing mangrove and non-mangrove areas.

Lastly, we trained a Support Vector Machine (SVM) model (Cortes & Vapnik, 1995), a supervised learning algorithm that constructs a hyperplane to optimally separate data into distinct classes. We implemented the SVM classifier using a Radial Basis Function (RBF) kernel, which is well-suited for capturing non-linear relationships in the data. Two key hyperparameters were tuned: gamma, which controls the influence of individual training examples (with lower values corresponding to broader influence), and cost, which balances the trade-off between maximizing the decision margin and minimizing classification error. A grid search was performed over 32 hyperparameter combinations, testing gamma values of 0.1, 0.3, 0.5, and 0.7, and cost values of 0.01, 0.1, 1, 10, 25, 50, 75, and 100. Each combination was trained on the training set and evaluated on the testing set, with accuracy scores recorded for comparison. Based on these results, the optimal configuration for the final SVM model was gamma = 0.1 and cost = 10.

4.6 Results

Our test and validation accuracy varied by the method used for the final CART, RF, and SVM models (Table 4.2). Based on the comparative performance of the three models, we selected the Random Forest (RF) classifier for extent mapping. We assessed the Random Forest model on the validation subset withheld during training. The confusion matrix for this subset resulted in an overall accuracy of 99.44% and a Kappa coefficient of 0.79, indicating strong agreement between predicted and actual land cover classes. Following this, the final model was applied to classify the

full 2020 Landsat image stack over the region of interest. The resulting classification output was post-processed using a connected pixel filter to remove isolated misclassified pixels. Only clusters with at least 50 connected pixels were preserved in the final map. To assess spatial performance at the pixel level, we compared the model's mangrove classification (binary: 1 = mangrove, 0 = non-mangrove) with GMW 2020 for the same region. From this spatial comparison, the model correctly identified 14,174 mangrove pixels (true positives) and approximately 2,286,057 nonmangrove pixels (true negatives). It misclassified 10,148 non-mangrove pixels as mangroves (false positives) and failed to detect 2,806 mangrove pixels (false negatives). The overall accuracy was calculated to be 99.44%, reflecting the proportion of all correctly classified pixels. To provide a clearer picture of model performance for the mangrove class, we also computed user's accuracy (precision) and producer's accuracy (recall). The user's accuracy was 58.28%, indicating that more than half of the pixels predicted as mangrove were correct. In contrast, the producer's accuracy was 83.47%, suggesting that most actual mangrove pixels were successfully identified. These metrics highlight a common trade-off: while the model tends to overpredict mangroves (resulting in a lower precision), it rarely fails to detect true mangrove areas (reflected in the high recall). Figure 4.6 presents the results of the 2020 classification, comparing the predicted mangrove extent generated by the Random Forest model with the known extent from the GMW dataset to visually assess spatial agreement.

We use the final Random Forest classifier to predict mangrove extent for each year from 1985 to 2020. To estimate total mangrove area, we calculate the number of pixels classified as mangroves and multiply by their actual ground area, converting the results to hectares. While year-to-year variation is evident in Figure 4.7, the overall trend indicates a steady increase in mangrove coverage across the region after 1990. A notable exception is the sharp decline between 1989 and

1990, which may be attributed to the extreme freeze event recorded during the 1989 Christmas period. Reports suggests that this cold snap brought sustained freezing temperatures across Florida, leading to widespread mangrove defoliation and dieback (Southeast Florida Coastal Marine Ecosystem, 2013).

4.7 Discussion

Annual maps of mangrove extent were generated from satellite imagery using GEE and machine learning models, addressing a key data gap in coastal ecosystem monitoring. This annual classification enables clearer tracking of mangrove change over time and supports analyses that align with policy interventions, disturbance events, and shifts in land use. Unlike existing global datasets limited to a few discrete years, the method developed here produces consistent annual classifications using multi-band Landsat imagery, spectral indices, and elevation data.

The Random Forest model achieves an overall validation accuracy of 89.65% in predicting mangrove extent, demonstrating strong performance in terms of both accuracy and recall. It effectively captures the spatial distribution of mangroves across the region, particularly in areas of persistent mangrove presence. However, the model exhibits a lower precision, indicating a tendency to misclassify certain non-mangrove areas as mangroves. Future work will explore the use of seasonal and tide-specific composites to better capture phenological and hydrological variation. In the future work, we also plan to explore deep learning approaches, particularly convolutional neural networks (CNNs) such as U-Net (Ronneberger et al., 2015), which may offer advantages in modeling complex spatial patterns and capturing finer structural details in coastal landscapes. U-Net is specifically designed for semantic segmentation and is well-suited to

preserving edge information and spatial coherence, which could potentially enhance the detection of fringe and narrow mangrove patches and reduce misclassification errors.

With this newly generated, annual mangrove extent dataset, we are now able to examine how changes in mangrove coverage translate into economic outcomes over time. Specifically, the data allows us to evaluate whether, and to what extent, the protective services provided by mangroves are reflected in housing market behavior. By aligning year-by-year mangrove extent with property transaction data, we can assess how proximity to mangroves and changes in their presence affect property values. This level of temporal and spatial resolution was not previously available and enhances our ability to investigate how the economic value of ecosystem services evolves alongside changes in ecological conditions.

Beyond its use in economic analysis, this dataset can support a range of applications in environmental and policy research. It allows tracking ecological responses to natural disturbances such as hurricanes, studying biodiversity, and monitoring vegetation change over time. It can also be linked with species richness and land cover data, making it useful for ecological and conservation planning. The classification outputs provide a foundation not only for valuing coastal protection services but also for broader research on ecosystem change and resilience. The underlying approach offers a scalable method for mapping mangrove extent that can be applied in other coastal regions.

Table 4.1: Indices Computed

Spectral	Type	Computation			
Indices		_			
NDVI		NIR – Red			
EVI		$\frac{\overline{NIR + Red}}{2.5 * (NIR - Red)}$			
SAVI	Vegetation Index	NIR + 6 * Red - 7.5 * Blue + 1 1.5 * (NIR - Red)			
GCVI		$NIR + Red + 0.5 \ \left(rac{NIR}{Green} ight) - 1$			
NDWI		Green – NIR			
MNDWI	Water Index	Green + NIR Green – SWIR			
LSWI		$Green + SWIR$ $NIR - SWIR$ $\overline{NIR + SWIR}$			
CMRI		NDVI - NDWI			
MMRI	Mangrove	(MNDWI - NDVI)			
	Index	$\frac{(MNDWI + NDVI)}{(MNDWI + NDVI)}$			
EBBI	Built-up Index	(SWIR - NIR)			
		$(10 * \sqrt{(SWIR + TIR)})$			
SR		NIR			
Ratio 5/4	Spectral Ratio	Red SWIR			
Ratio 3/5		NIR Red			
		SWIR			

Table 4.2: Model Outcome

Model	CART	RF	SVM
Test Accuracy (%)	92.00	92.90	92.80
Validation Accuracy (%)	88.96	89.65	88.52
Kappa (%)	78.00	79.00	77.00
Overall Accuracy (%)	99.36	99.44	99.43
User Accuracy (%)	54.28	58.28	57.48
Producer Accuracy (%)	84.92	83.47	83.30

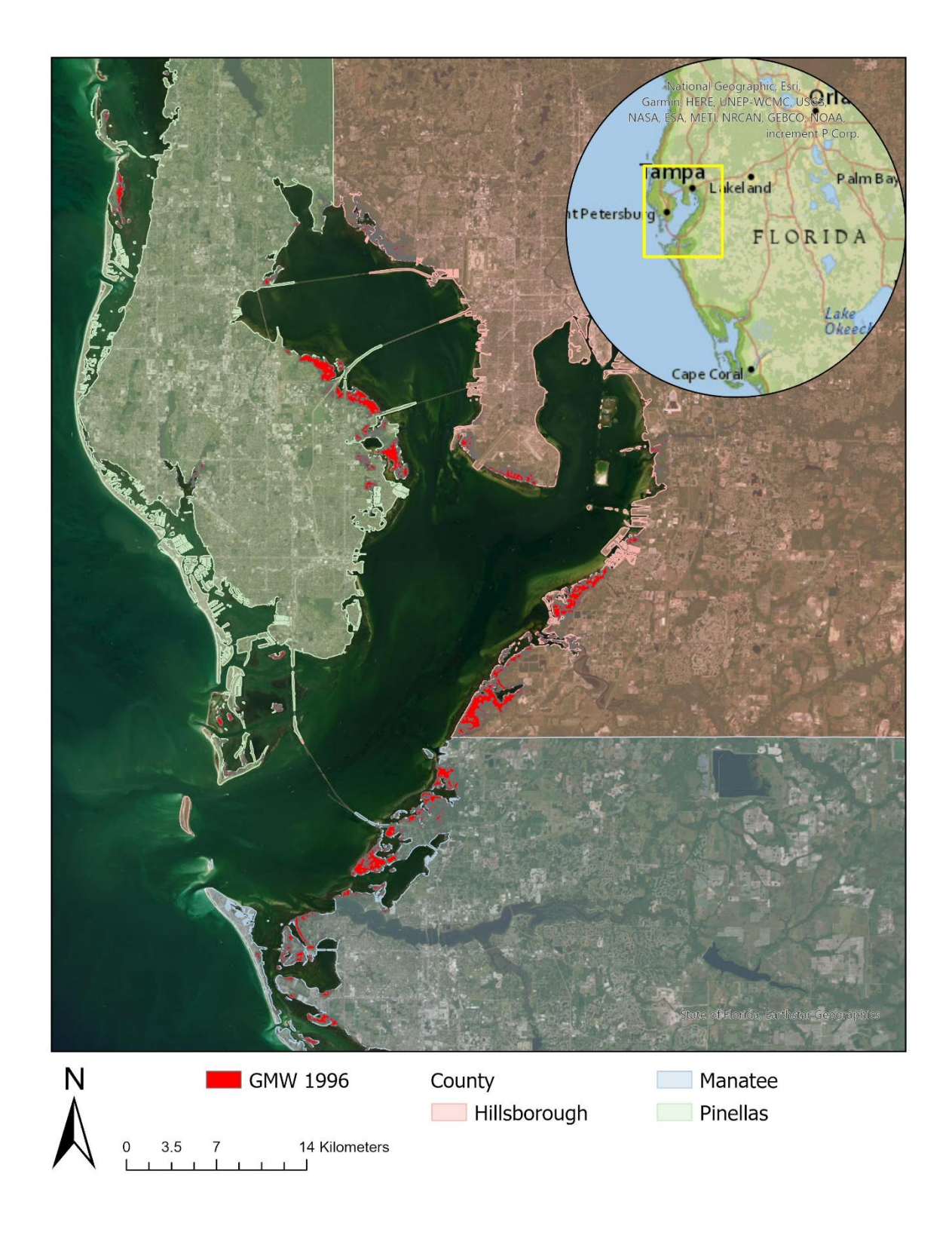


Figure 4.1: Study Area: Tampa Bay, Southwest Florida

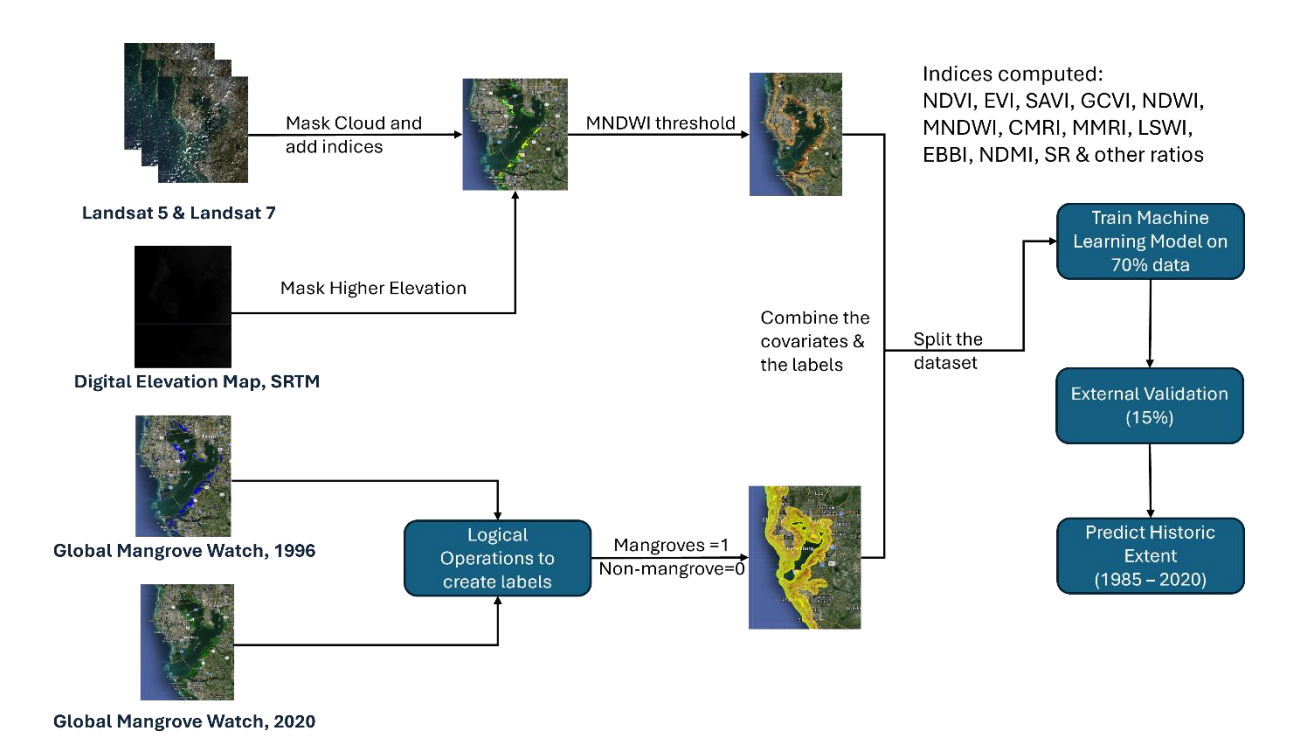


Figure 4.2: Block Diagram of Mangroves Extent Mapping

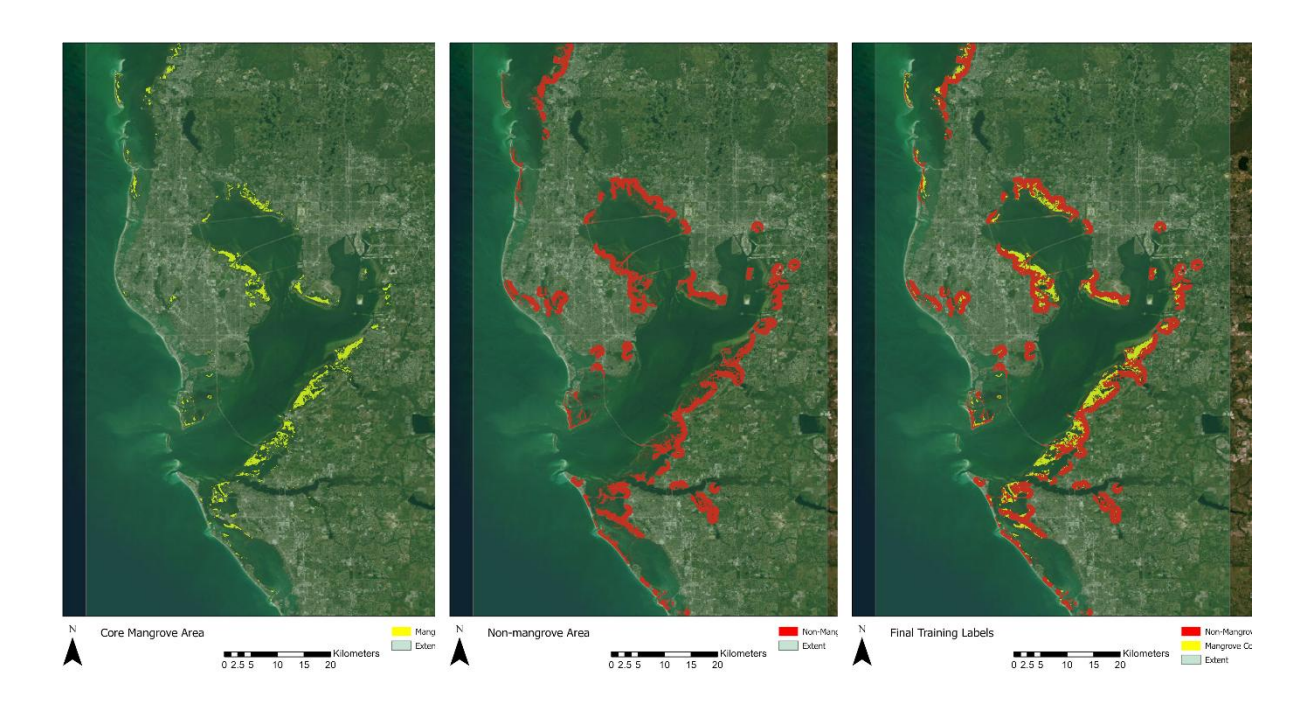


Figure 4.3: Spatial distribution of (a) core mangrove areas, (b) non-mangrove regions, and (c) final training labels used for classification.

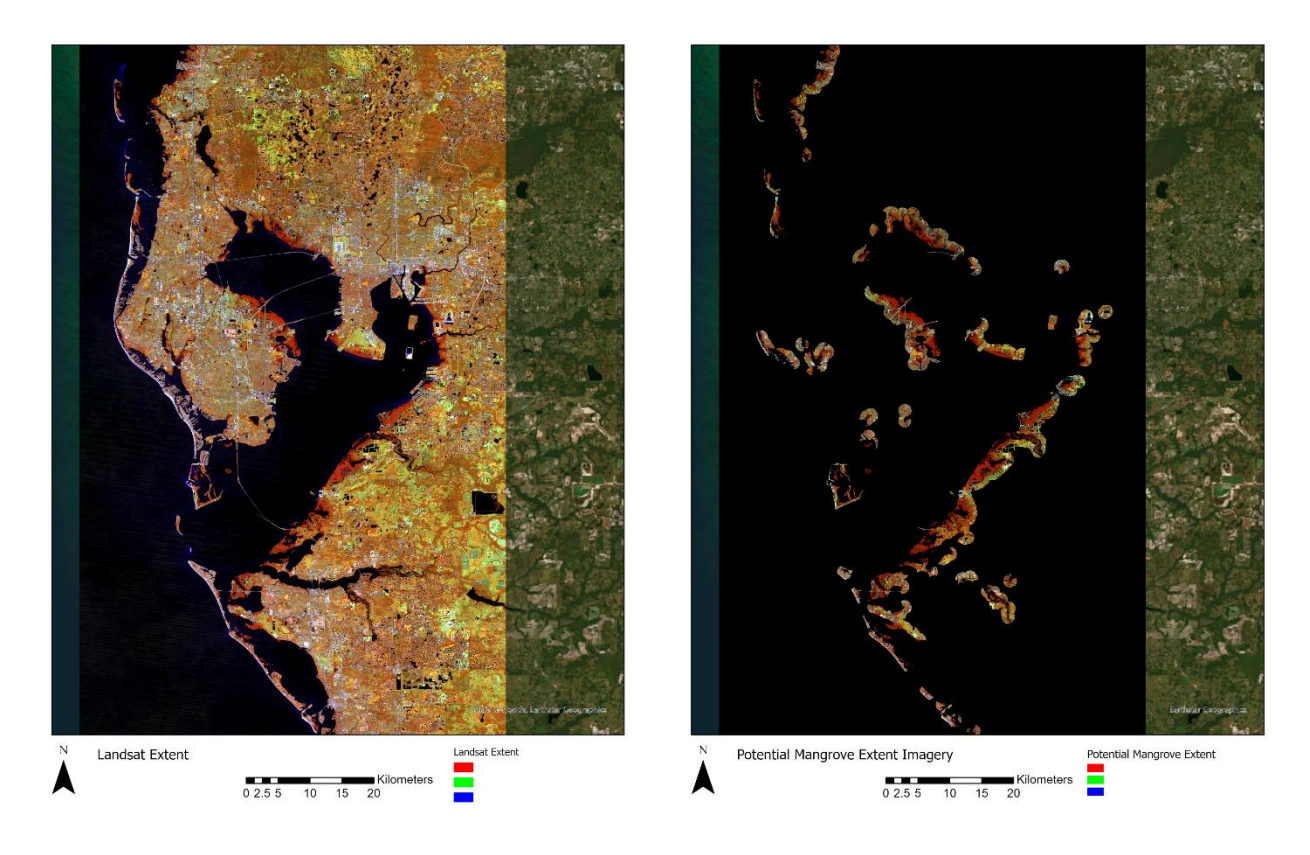


Figure 4.4: Pre-processed and Final Landsat surface reflectance image for the year 2020

Note: (a) Pre-processed Landsat surface reflectance image for the year 2020, including cloud masking and scaling. (b) Final image stack used for classification, incorporating spectral indices and elevation data, clipped to the area of interest.

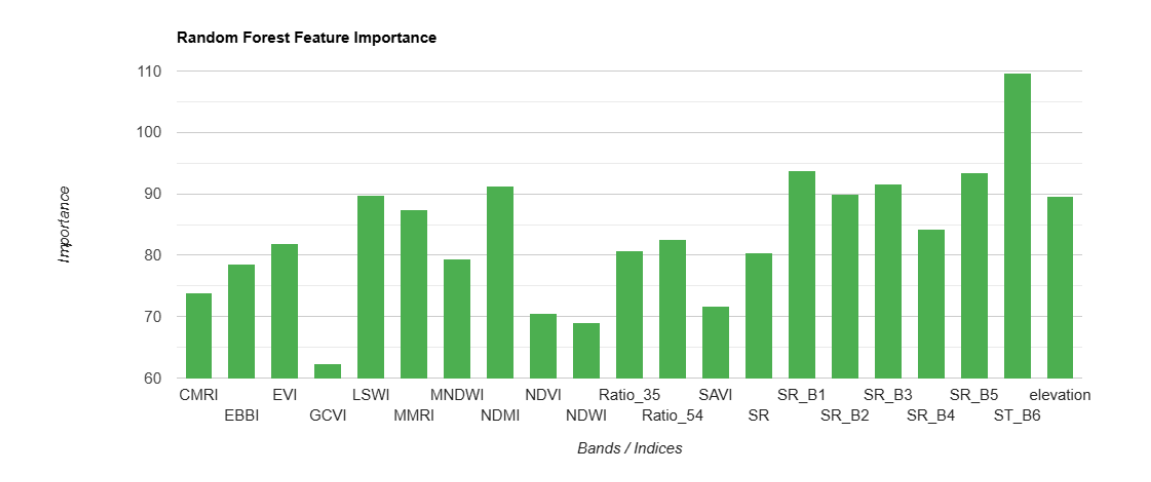


Figure 4.5: Variable Importance from Random Forest Classifier

Note: The surface reflectance band 6 (ST_B6), which corresponds to the thermal infrared (TIR) portion of the electromagnetic spectrum (10.4– $12.5~\mu m$), emerged as the most influential predictor, followed by SR_B1 (blue, 0.45– $0.52~\mu m$), SR_B5 (short-wave infrared, 1.55– $1.75~\mu m$), SR_B3 (red, 0.63– $0.69~\mu m$), the Normalized Difference Moisture Index (NDMI) and the elevation.

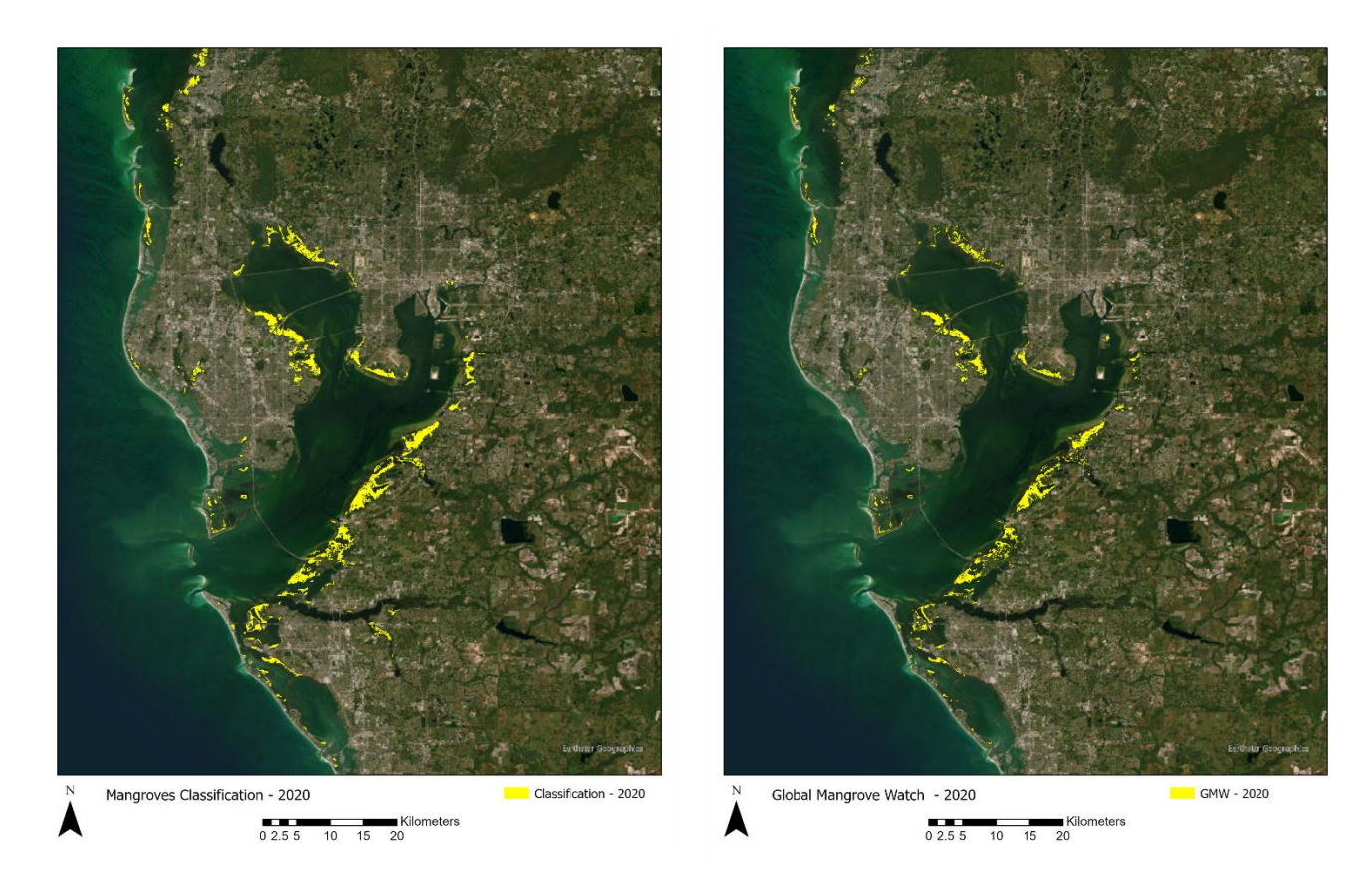


Figure 4.6: Predicted mangrove extent and GMW mangrove extent for 2020

Note: (a) Predicted mangrove extent for 2020 based on RF classification; (b) known GMW mangrove extent for 2020. To better understand which variables contributed most to the Random Forest classification, we examined the feature importance scores generated by the model. As shown in Figure 4.6, the surface reflectance band 6 (ST_B6) emerged as the most influential predictor, followed by SR_B1, SR_B5, SR_B3, NDMI and elevation. These results highlight the importance of spectral and hydrological indicators in distinguishing mangrove and non-mangrove areas.

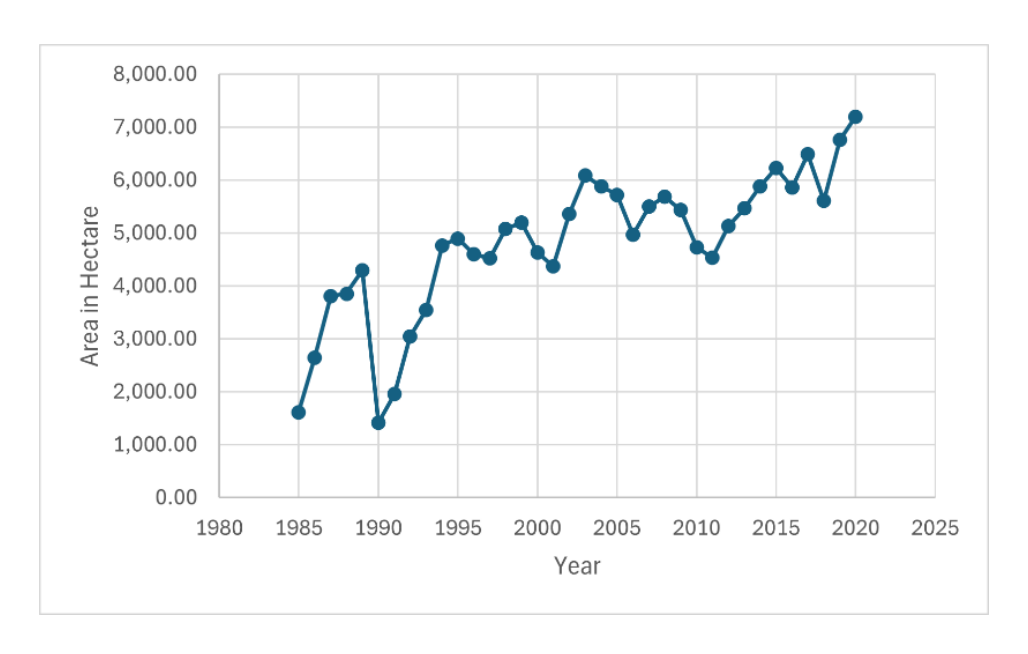


Figure 4.7: Predicted mangroves year on year

Note: The overall trend indicates a steady increase in mangrove coverage across the region after 1990. A notable exception is the sharp decline between 1989 and 1990, which may be attributed to the extreme freeze event recorded during the 1989 Christmas period. Reports suggests that this cold snap brought sustained freezing temperatures across Florida, leading to widespread mangrove defoliation and dieback (Southeast Florida Coastal Marine Ecosystem, 2013).

Chapter 5

Conclusion

Together, the three chapters in this dissertation offer complementary perspectives on the economic value of mangrove ecosystems in coastal Florida. The first chapter captures the salience of mangrove protection in the immediate aftermath of a hurricane, providing evidence of how natural defenses are perceived during extreme weather events. The second chapter moves beyond disaster contexts to examine whether mangrove presence is consistently valued in property markets over longer time horizons. The third chapter addresses a key data limitation by reconstructing historical mangrove extent using remote sensing and machine learning, offering a foundation for future long-term valuation studies. Collectively, these studies contribute to a deeper understanding of how protective ecosystem services are reflected in market behavior and underscore the importance of integrating natural infrastructure into coastal resilience planning and economic decision-making.

REFERENCES

- Alongi, D. M. (2008). Mangrove forests: Resilience, protection from tsunamis, and responses to global climate change. *Estuarine, Coastal and Shelf Science*, 76(1), 1–13. https://doi.org/10.1016/j.ecss.2007.08.024
- As-syakur, Abd. R., Adnyana, I. W. S., Arthana, I. W., & Nuarsa, I. W. (2012). Enhanced Built-Up and Bareness Index (EBBI) for Mapping Built-Up and Bare Land in an Urban Area. *Remote Sensing*, 4(10), 2957–2970. https://doi.org/10.3390/rs4102957
- Atreya, A., & Ferreira, S. (2015). Seeing is Believing? Evidence from Property Prices in Inundated Areas.

 Risk Analysis, 35(5), 828–848. https://doi.org/10.1111/risa.12307
- Atreya, A., Ferreira, S., & Kriesel, W. (2013). Forgetting the Flood? An Analysis of the Flood Risk Discount over Time. *Land Economics*, 89(4), 577–596. https://doi.org/10.3368/le.89.4.577
- Bakkensen, L. A., & Barrage, L. (2022). Going Underwater? Flood Risk Belief Heterogeneity and Coastal Home Price Dynamics. *The Review of Financial Studies*, *35*(8), 3666–3709. https://doi.org/10.1093/rfs/hhab122
- Bakkensen, L. A., Ding, X., & Ma, L. (2019). Flood Risk and Salience: New Evidence from the Sunshine State. *Southern Economic Journal*, 85(4), 1132–1158. https://doi.org/10.1002/soej.12327
- Barbier, E. B. (2007). Valuing ecosystem services as productive inputs. *Economic Policy*, 22(49), 178–229. https://doi.org/10.1111/j.1468-0327.2007.00174.x
- Barbier, E. B. (2008). In the wake of tsunami: Lessons learned from the household decision to replant mangroves in Thailand. *Resource and Energy Economics*, 30(2), 229–249. https://doi.org/10.1016/j.reseneeco.2007.08.002

- Barbier, E. B., & Enchelmeyer, B. S. (2014). Valuing the storm surge protection service of US Gulf Coast wetlands. *Journal of Environmental Economics and Policy*, *3*(2), 167–185. https://doi.org/10.1080/21606544.2013.876370
- Barbier, E. B., Georgiou, I. Y., Enchelmeyer, B., & Reed, D. J. (2013). The Value of Wetlands in Protecting Southeast Louisiana from Hurricane Storm Surges. *PLoS ONE*, 8(3), e58715. https://doi.org/10.1371/journal.pone.0058715
- Bin, O., Crawford, T. W., Kruse, J. B., & Landry, C. E. (2008). Viewscapes and Flood Hazard: Coastal Housing Market Response to Amenities and Risk. *Land Economics*, 84(3), 434–448. https://doi.org/10.3368/le.84.3.434
- Bin, O., Kruse, J. B., & Landry, C. E. (2008). Flood Hazards, Insurance Rates, and Amenities: Evidence From the Coastal Housing Market. *Journal of Risk and Insurance*, 75(1), 63–82. https://doi.org/10.1111/j.1539-6975.2007.00248.x
- Breiman, L. (2001). Random forests. Machine Learning.
- Breiman, L., Friedman, J., Olshen, R. A., & Stone, C. J. (1984). *Classification and regression trees.*Routledge. (1st ed.).
- Bunting, P., Rosenqvist, A., Hilarides, L., Lucas, R. M., Thomas, N., Tadono, T., Worthington, T. A., Spalding, M., Murray, N. J., & Rebelo, L.-M. (2022). Global Mangrove Extent Change 1996–2020: Global Mangrove Watch Version 3.0. *Remote Sensing*, *14*(15), 3657. https://doi.org/10.3390/rs14153657
- Bunting, P., Rosenqvist, A., Lucas, R. M., Rebelo, L.-M., Hilarides, L., Thomas, N., Hardy, A., Itoh, T., Shimada, M., & Finlayson, C. M. (2018). The Global Mangrove Watch—A New 2010 Global Baseline of Mangrove Extent. *Remote Sensing*, 10(10), 1669. https://doi.org/10.3390/rs10101669
- Canny, J. (1986). A Computational Approach to Edge Detection. *IEEE Transactions on Pattern Analysis* and Machine Intelligence, PAMI-8(6), 679–698. https://doi.org/10.1109/TPAMI.1986.4767851

- Chandrasekar, K., Sesha Sai, M. V. R., Roy, P. S., & Dwevedi, R. S. (2010). Land Surface Water Index (LSWI) response to rainfall and NDVI using the MODIS Vegetation Index product. *International Journal of Remote Sensing*, 31(15), 3987–4005. https://doi.org/10.1080/01431160802575653
- Chay, K. Y., & Michael, G. (2005). Does Air Quality Matter? Evidence from the Housing Market. *Journal of Political Economy*, 113(2), 376–424.
- Chen, Q., Li, Y., Kelly, D. M., Zhang, K., Zachry, B., & Rhome, J. (2021). Improved modeling of the role of mangroves in storm surge attenuation. *Estuarine, Coastal and Shelf Science*, 260, 107515. https://doi.org/10.1016/j.ecss.2021.107515
- Cortes, C., & Vapnik, V. (1995). Support-vector networks. *Machine Learning*, 20(3), 273–297. https://doi.org/10.1007/BF00994018
- Danielsen, F., Sørensen, M. K., Olwig, M. F., Selvam, V., Parish, F., Burgess, N. D., Hiraishi, T.,
 Karunagaran, V. M., Rasmussen, M. S., Hansen, L. B., Quarto, A., & Suryadiputra, N. (2005).
 The Asian Tsunami: A Protective Role for Coastal Vegetation. *Science*, 310(5748), 643–643.
 https://doi.org/10.1126/science.1118387
- Das, S., & Crépin, A.-S. (2013). Mangroves can provide protection against wind damage during storms. *Estuarine, Coastal and Shelf Science*, 134, 98–107. https://doi.org/10.1016/j.ecss.2013.09.021
- Das, S., & Vincent, J. R. (2009). Mangroves protected villages and reduced death toll during Indian super cyclone. *Proceedings of the National Academy of Sciences*, *106*(18), 7357–7360. https://doi.org/10.1073/pnas.0810440106
- DasGupta, R., & Shaw, R. (Eds.). (2017). *Participatory Mangrove Management in a Changing Climate*. Springer Japan. https://doi.org/10.1007/978-4-431-56481-2
- Del Valle, A., Eriksson, M., Ishizawa, O. A., & Miranda, J. J. (2020). Mangroves protect coastal economic activity from hurricanes. *Proceedings of the National Academy of Sciences*, 117(1), 265–270. https://doi.org/10.1073/pnas.1911617116

- Diniz, C., Cortinhas, L., Nerino, G., Rodrigues, J., Sadeck, L., Adami, M., & Souza-Filho, P. W. M. (2019). Brazilian Mangrove Status: Three Decades of Satellite Data Analysis. *Remote Sensing*, 11(7), 808. https://doi.org/10.3390/rs11070808
- Donchyts, G., Schellekens, J., Winsemius, H., Eisemann, E., & Van De Giesen, N. (2016). A 30 m

 Resolution Surface Water Mask Including Estimation of Positional and Thematic Differences

 Using Landsat 8, SRTM and OpenStreetMap: A Case Study in the Murray-Darling Basin,

 Australia. *Remote Sensing*, 8(5), 386. https://doi.org/10.3390/rs8050386
- Dundas, S. J. (2017a). Benefits and ancillary costs of natural infrastructure: Evidence from the New Jersey coast. *Journal of Environmental Economics and Management*, 85, 62–80. https://doi.org/10.1016/j.jeem.2017.04.008
- Dundas, S. J. (2017b). Benefits and ancillary costs of natural infrastructure: Evidence from the New Jersey coast. *Journal of Environmental Economics and Management*, 85, 62–80. https://doi.org/10.1016/j.jeem.2017.04.008
- Farr, T. G., Rosen, P. A., Caro, E., Crippen, R., Duren, R., Hensley, S., Kobrick, M., Paller, M., Rodriguez, E., Roth, L., Seal, D., Shaffer, S., Shimada, J., Umland, J., Werner, M., Oskin, M., Burbank, D., & Alsdorf, D. (2007). The Shuttle Radar Topography Mission. *Reviews of Geophysics*, 45(2), 2005RG000183. https://doi.org/10.1029/2005RG000183
- Federal Emergency Management Agency (FEMA). (2018). *Hurricane Season FEMA After-Action Report*.

 U.S. Department of Homeland Security. https://www.fema.gov/sites/default/files/2020-08/fema hurricane-season-after-action-report 2017.pdf
- Flooding Facts. (2024, November 18). ArcGIS StoryMaps.

 https://storymaps.arcgis.com/collections/66b8cb55c0d84bb4b69e92d7f473a624
- Flooding Information—Irma. (n.d.). Lee County Southwest Florida. Retrieved July 7, 2025, from https://www.leegov.com:443/flooding/irma

- Florida Department of Environmental Protection. (2024). *Florida's Mangroves*. Florida Department of Environmental Protection. https://floridadep.gov/rcp/rcp/content/floridas-mangroves
- Ganjirad, M., & Bagheri, H. (2024). Google Earth Engine-based mapping of land use and land cover for weather forecast models using Landsat 8 imagery. *Ecological Informatics*, 80, 102498. https://doi.org/10.1016/j.ecoinf.2024.102498
- Gao, B. (1996). NDWI—A normalized difference water index for remote sensing of vegetation liquid water from space. *Remote Sensing of Environment*, *58*(3), 257–266. https://doi.org/10.1016/S0034-4257(96)00067-3
- Garcia, L., Anastasiou, C., & Robison, D. (2023). *Tampa Bay Surface Water Improvement and Management (SWIM) Plan Update* (p. 112). Southwest Florida Water Management District.
- Giri, C., Ochieng, E., Tieszen, L. L., Zhu, Z., Singh, A., Loveland, T., Masek, J., & Duke, N. (2011).
 Status and distribution of mangrove forests of the world using earth observation satellite data.
 Global Ecology and Biogeography, 20(1), 154–159. https://doi.org/10.1111/j.1466-8238.2010.00584.x
- Gitelson, A. A., Viña, A., Arkebauer, T. J., Rundquist, D. C., Keydan, G., & Leavitt, B. (2003). Remote estimation of leaf area index and green leaf biomass in maize canopies. *Geophysical Research Letters*, 30(5), 2002GL016450. https://doi.org/10.1029/2002GL016450
- Gopalakrishnan, S., Smith, M. D., Slott, J. M., & Murray, A. B. (2011). The value of disappearing beaches: A hedonic pricing model with endogenous beach width. *Journal of Environmental Economics and Management*, 61(3), 297–310. https://doi.org/10.1016/j.jeem.2010.09.003
- Gorelick, N., Hancher, M., Dixon, M., Ilyushchenko, S., Thau, D., & Moore, R. (2017). Google Earth Engine: Planetary-scale geospatial analysis for everyone. *Remote Sensing of Environment*, 202, 18–27. https://doi.org/10.1016/j.rse.2017.06.031

- Guo, M., Yu, Z., Xu, Y., Huang, Y., & Li, C. (2021). ME-Net: A Deep Convolutional Neural Network for Extracting Mangrove Using Sentinel-2A Data. *Remote Sensing*, 13(7), 1292. https://doi.org/10.3390/rs13071292
- Gupta, K., Mukhopadhyay, A., Giri, S., Chanda, A., Datta Majumdar, S., Samanta, S., Mitra, D., Samal,
 R. N., Pattnaik, A. K., & Hazra, S. (2018). An index for discrimination of mangroves from non-mangroves using LANDSAT 8 OLI imagery. *MethodsX*, 5, 1129–1139.
 https://doi.org/10.1016/j.mex.2018.09.011
- Hallstrom, D. G., & Smith, V. K. (2005). Market responses to hurricanes. *Journal of Environmental Economics and Management*, 50(3), 541–561. https://doi.org/10.1016/j.jeem.2005.05.002
- Hamilton, S. E., & Morgan, A. (2010). Integrating lidar, GIS and hedonic price modeling to measure amenity values in urban beach residential property markets. *Computers, Environment and Urban Systems*, 34(2), 133–141. https://doi.org/10.1016/j.compenvurbsys.2009.10.007
- Hashida, Y., & Dundas, S. J. (2023). The effects of a voluntary property buyout and acquisition program on coastal housing markets: Evidence from New York. *Journal of Environmental Economics and Management*, 121, 102873. https://doi.org/10.1016/j.jeem.2023.102873
- Hochard, J. P., Barbier, E. B., & Hamilton, S. E. (2021). Mangroves and coastal topography create economic "safe havens" from tropical storms. *Scientific Reports*, *11*(1), 15359. https://doi.org/10.1038/s41598-021-94207-3
- Hochard, J. P., Hamilton, S., & Barbier, E. B. (2019). Mangroves shelter coastal economic activity from cyclones. *Proceedings of the National Academy of Sciences*, *116*(25), 12232–12237. https://doi.org/10.1073/pnas.1820067116
- Huete, A., Didan, K., Leeuwen, W. V., Jacobson, A., Solanos, R., & Laing, T. (1999). Modis Vegetation

 Index (MOD 13) Algorithm Theoretical Basis Document.
- Huete, A. R. (1988). A soil-adjusted vegetation index (SAVI). *Remote Sensing of Environment*, 25(3), 295–309. https://doi.org/10.1016/0034-4257(88)90106-X

- Iii, J. W. B., & Walker, T. (2016). Total ecosystem services values (TEV) in southwest Florida: The ECOSERVE method. *Florida Scientist*.
- Jordan, C. F. (1969). Derivation of Leaf-Area Index from Quality of Light on the Forest Floor. *Ecology*, 50(4), 663–666. https://doi.org/10.2307/1936256
- Kousky, C. (2019). The Role of Natural Disaster Insurance in Recovery and Risk Reduction. *Annual Review of Resource Economics*, 11(1), 399–418. https://doi.org/10.1146/annurev-resource-100518-094028
- Kuminoff, N. V., Parmeter, C. F., & Pope, J. C. (2010). Which hedonic models can we trust to recover the marginal willingness to pay for environmental amenities? *Journal of Environmental Economics* and Management, 60(3), 145–160. https://doi.org/10.1016/j.jeem.2010.06.001
- Lagomasino, D., Fatoyinbo, T., Castañeda-Moya, E., Cook, B. D., Montesano, P. M., Neigh, C. S. R., Corp, L. A., Ott, L. E., Chavez, S., & Morton, D. C. (2021). Storm surge and ponding explain mangrove dieback in southwest Florida following Hurricane Irma. *Nature Communications*, 12(1), 4003. https://doi.org/10.1038/s41467-021-24253-y
- Landry, C. E., & Hindsley, P. (2021). Valuing Beach Quality with Hedonic Property Models.
- Livy, M. R., & Klaiber, H. A. (2016). Maintaining Public Goods: The Capitalized Value of Local Park Renovations. *Land Economics*, 92(1), 96–116. https://doi.org/10.3368/le.92.1.96
- M, A., Ahmed, S. A., & N, H. (2023). Land use and land cover classification using machine learning algorithms in google earth engine. *Earth Science Informatics*, *16*(4), 3057–3073. https://doi.org/10.1007/s12145-023-01073-w
- Mangrove Trimming and Preservation Act, Pub. L. No. 403.9321–403.9333 (1996).
- Maza, M., Adler, K., Ramos, D., Garcia, A. M., & Nepf, H. (2017). Velocity and Drag Evolution From the Leading Edge of a Model Mangrove Forest. *Journal of Geophysical Research: Oceans*, 122(11), 9144–9159. https://doi.org/10.1002/2017JC012945

- Menéndez, P., Losada, I. J., Torres-Ortega, S., Narayan, S., & Beck, M. W. (2020). The Global Flood

 Protection Benefits of Mangroves. *Scientific Reports*, 10(1), 4404.

 https://doi.org/10.1038/s41598-020-61136-6
- Millennium Ecosystem Assessment (Ed.). (2005). *Ecosystems and human well-being: Synthesis*. Island Press.
- Narayan, S., Thomas, C., Matthewman, J., Shepard, C. C., Geselbracht, L., Nzerem, K., & Beck, M. W. (2019). *Valuing the Flood Risk Reduction Benefits of Florida's Mangroves*.
- NASA Jet Propulsion Laboratory. (2013). SRTM Plus Version 3 Digital Elevation Model, 1 arc-second resolution [Dataset]. https://doi.org/10.5067/MEaSUREs/SRTM/SRTMGL1.003
- National Oceanic and Atmospheric Administration, Office for Coastal Management. (2013). *National Coastal Population Report: Population Trends from 1970 to 2020*. chrome-extension://efaidnbmnnnibpcajpcglclefindmkaj/https://cdn.oceanservice.noaa.gov/oceanserviceprod/facts/coastal-population-report.pdf
- Otsu, N. (1979). A Threshold Selection Method from Gray-Level Histograms.
- Palmquist, R. B. (1982). Measuring environmental effects on property values without hedonic regressions. *Journal of Urban Economics*, 11(3), 333–347. https://doi.org/10.1016/0094-1190(82)90079-1
- Paterson, R. W., & Boyle, K. J. (2002). Out of Sight, Out of Mind? Using GIS to Incorporate Visibility in Hedonic Property Value Models. *Land Economics*, 78(3), 417–425. https://doi.org/10.2307/3146899
- Ronneberger, O., Fischer, P., & Brox, T. (2015). U-Net: Convolutional Networks for Biomedical Image Segmentation. In N. Navab, J. Hornegger, W. M. Wells, & A. F. Frangi (Eds.), *Medical Image Computing and Computer-Assisted Intervention MICCAI 2015* (Vol. 9351, pp. 234–241). Springer International Publishing. https://doi.org/10.1007/978-3-319-24574-4_28

- Sander, H. A., & Polasky, S. (2009). The value of views and open space: Estimates from a hedonic pricing model for Ramsey County, Minnesota, USA. *Land Use Policy*, 26(3), 837–845. https://doi.org/10.1016/j.landusepol.2008.10.009
- Southeast Florida Coastal Marine Ecosystem. (2013). Shoreline Habitat: Mangroves. —MARine and
 Estuarine goal Setting for South Florida. chromeextension://efaidnbmnnnibpcajpcglclefindmkaj/https://www.aoml.noaa.gov/ocd/ocdweb/docs/M
 ARES/MARES_SEFC_ICEM__20131001_Appendix_Mangroves.pdf
- Sun, F., & Carson, R. T. (2020). Coastal wetlands reduce property damage during tropical cyclones.
 Proceedings of the National Academy of Sciences, 117(11), 5719–5725.
 https://doi.org/10.1073/pnas.1915169117
- Tarpley, J. D., Schneider, S. R., & Money, R. L. (1984). Global Vegetation Indices from the NOAA-7 Meteorological Satellite. *Journal of Climate and Applied Meteorology*, 23(3), 491–494. https://doi.org/10.1175/1520-0450(1984)023<0491:GVIFTN>2.0.CO;2
- Taylor, C. A., & Druckenmiller, H. (2022). Wetlands, Flooding, and the Clean Water Act. *American Economic Review*, *112*(4), 1334–1363. https://doi.org/10.1257/aer.20210497
- Temmerman, S., Horstman, E. M., Krauss, K. W., Mullarney, J. C., Pelckmans, I., & Schoutens, K. (2023). Marshes and Mangroves as Nature-Based Coastal Storm Buffers. *Annual Review of Marine Science*, *15*(1), 95–118. https://doi.org/10.1146/annurev-marine-040422-092951
- Tomiczek, T., Wargula, A., Hurst, N., Bryant, D., & Provost, L. (2021). *Engineering With Nature: The role of mangroves in coastal protection*. Engineer Research and Development Center (U.S.). https://doi.org/10.21079/11681/42420
- US EPA, O. (2016, June 27). Climate Change Indicators: Tropical Cyclone Activity [Reports and Assessments]. https://www.epa.gov/climate-indicators/climate-change-indicators-tropical-cyclone-activity

- U.S. Geological Survey. (2020a). Landsat 5 TM Collection 2 Tier 1 Level-2 Surface Reflectance and Surface Temperature [Dataset]. https://developers.google.com/earth-engine/datasets/catalog/LANDSAT LT05 C02 T1 L2
- U.S. Geological Survey. (2020b). Landsat 7 ETM+ Collection 2 Tier 1 Level-2 Surface Reflectance and Surface Temperature [Dataset]. https://developers.google.com/earth-engine/datasets/catalog/LANDSAT_LE07_C02_T1_L2
- Walls, M., Kousky, C., & Chu, Z. (2015). Is What You See What You Get? The Value of Natural Landscape Views.
- Xu, H. (2006). Modification of normalised difference water index (NDWI) to enhance open water features in remotely sensed imagery. *International Journal of Remote Sensing*, 27(14), 3025–3033. https://doi.org/10.1080/01431160600589179
- Yancho, J., Jones, T., Gandhi, S., Ferster, C., Lin, A., & Glass, L. (2020). The Google Earth Engine Mangrove Mapping Methodology (GEEMMM). *Remote Sensing*, 12(22), 3758. https://doi.org/10.3390/rs12223758
- Yang, M., Mou, Y., Liu, S., Meng, Y., Liu, Z., Li, P., Xiang, W., Zhou, X., & Peng, C. (2022). Detecting and mapping tree crowns based on convolutional neural network and Google Earth images.

 International Journal of Applied Earth Observation and Geoinformation, 108, 102764.

 https://doi.org/10.1016/j.jag.2022.102764
- Zhang, K., Liu, H., Li, Y., Xu, H., Shen, J., Rhome, J., & Smith, T. J. (2012). The role of mangroves in attenuating storm surges. *Estuarine, Coastal and Shelf Science*, 102–103, 11–23. https://doi.org/10.1016/j.ecss.2012.02.021